UNIVERSITY OF CRETE

MATERIALS SCIENCE AND TECHNOLOGY DEPARTMENT

Rearrangements of PMMA hard sphere glasses investigated by LAOS and Echo-DWS

Marios Savvakis

Supervisor: George Petekidis

FOUNDATION FOR RESEACH AND TECHNOLOGY

INSTITUTE OF ELECTRONIC STRUCTURE AND LASER

HERAKLION CRETE, JULY 2015

Chapter 1: Introduction

A **colloid** is a substance in which microscopically dispersed insoluble particles are suspended throughout another substance. When colloids are suspended in a medium, they form a suspension. The term suspension refers to mixtures where the colloids size are less than the dispersed phase particles. On the other hand when the colloids size is greater than the dispersed phase particles, then the term dispersion is used. Size range deviates from nm (10^{-9}m) to mm (10^{-6}m). The mass of the colloid ought to be significantly larger than the mass of the suspending fluid molecules, this is critical so that the suspending medium can be considered continuum on the length scale and time scale of colloidal motion. Moreover, the upper size limit makes sure that thermal forces are still of importance, while the gravitational forces are not able to remove particles from the dispersion.

Brownian motion theory: The theory of Brownian motion was elucidated separately by Albert Einstein and by Marian von Smoluchowski. The equation can relate the mean square displacement of the colloidal particle, with the time allowed for diffusion:

$$\lim_{t\to\infty} \langle (\Delta r(t))^2 \rangle = 6Dt$$

Where the D coefficient is the **Einstein- Smoluchowski diffusivity**. It was calculated by Sutherland and Einstein separately. For a spherical shaped colloid, we have:

$$D_0 = \frac{K_B T}{6\pi\eta R}$$

Which is known as the **Stokes-Einstein-Sutherland** equation.

Perrin observed the random diffusion of individual particles and showed that their Brownian motions are just large scale manifestations of the thermal motions of atoms. The experiments he did, verified that the equipartition of energy is obeyed by the particles. The average kinetic energy of each particle is $\frac{3}{2}K_B T$, where K_B Boltzmann's constant is and T is temperature. All the states of atomic systems: gas, liquid, crystal, alloy and glass have analogues in Colloidal systems.

Colloidal systems mimic the behavior of atoms and as a result, they have special properties that allow experiments which would be difficult or even impossible to be done in atomic systems [2].

Colloidal interactions: When there are many particles, interactions arise between colloids, while the types of interactions are via surface, depletion, dispersion and hydrodynamic forces, with the difference being the source of the interactions.

When induced disturbance in the fluid flow field occurs by the presence of a particle, hydrodynamic interactions arise. In addition, surface forces are being introduced if the colloidal particles are in close proximity where the surfaces might be also charged by Ion absorption or in the case of grafted polymers.

Given potential of interaction Φ(r) which is a function of the distance r between the particle centers, we can calculate the force by derivation:

$$F(r) = -\frac{d\Phi(\mathrm{r})}{dr}$$

Molecules and atoms interact by dispersion forces as seen also in colloidal particles. Dispersion forces result from the polarization caused by the electron cloud of one atom with the fluctuating cloud of another.

The London-Van der Waals force between the particles actually consists the total effect of the fluctuating polarization. In the simplest case, the force between two homogenous plates in close approach, the dispersion potential of the interaction has the form of:

$$\frac{\Phi^d(h)}{area} = -\frac{A}{12\pi h^2}$$ (Per area of plate)

Where h is the distance between the particle surfaces, coefficient A is the hamaker constant. It is a function of the suspending medium and the type of material of the particles. The coefficient range is between $(30 * 10^{-20})$ J for gold particles in water, to (10^{-20}) J or less, for inorganic and polymeric particles.

If the surfaces touch, the dispersion potential is going to minus infinity, this suggests cold-wielding of the particles and, indeed, the Hamaker constant can be estimated from the work of adhesion.

For real particle systems, surface roughness, absorbed or chemically bound ions and solvent molecules on the surface affect particle aggregation.

Chapter 2: Background

2.1 Hard spheres model:

Hard spheres are used in the statistical theories of fluids and solids together, as model particles. They are impenetrable spheres that cannot overlap in space, while at the same time the strong repulsion that atoms and spherical molecules experience in very close distances is mimicked by them. These systems can be studied by computer dynamics simulation and experiments. Colloidal hard spheres are an ideal scenario of microscopic particles moving in a medium through Brownian motion and interacting with an infinite repulsive potential when they touch.

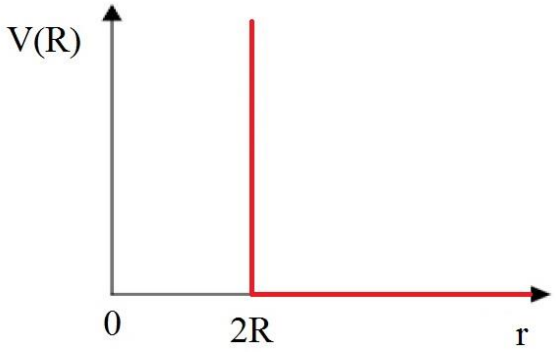

Figure 2.1.1: *hard sphere particles of radius R potential is depicted, with center to center separation r.*

The potential V(r) is ∞ when 0<r<2R and 0 when r>2R, where R is the particle radius. Only entropy is considered to determine phase behavior, since there are no enthalpic interactions. We can thus characterize this system by the number density of the particles alone. This is expressed in colloid volume fraction φ:

$$\varphi = \frac{4}{3}\pi R^3 \frac{N}{V}$$

Van der waals attractive forces may cause colloidal particles to aggregate irreversibly. This attraction has long range in order to be able to affect particles in the size of colloids. The strength of the resulting attractive potential is proportional to the refractive index mismatch between the solvent and the particle that could be as much

as many times that of the thermal energy. For this reason it is important that the colloids are stabilized in order to prevent aggregation.

Steric stabilization is the method used to stabilize the colloidal particles we used in this work. Polymer chains are grafted on the surface of colloidal particles, so that when two particles approach their chains both penetrate each other with the resulting entropy to be sufficiently lowered. As a result, a strong repulsion emerges between the two polymer layers and prevents the particles from getting close. With the correct grafting density and length of the polymer chains, the resulting potential is a good approximation of that of the hard spheres.

Hard spheres phase diagram: Hard spheres exhibit a liquid phase at volume fractions below of 49.4% where the given space to the particles is big enough for them to diffuse freely and explore the whole volume available. By increasing the volume fraction further the liquid and crystal coexist and between 49.4% and 54.5 %. The fully crystalline phase exists from 54.5% to 58%. Upon further incretion, the glass state is reached between 58% and 64%. Hard spheres cannot overlap, as a result the maximum packing in an ordered state is 74%, while in the case of an amorphous random close packed structure the maximum packing fraction is $\varphi_{RCP} = 0.64$.

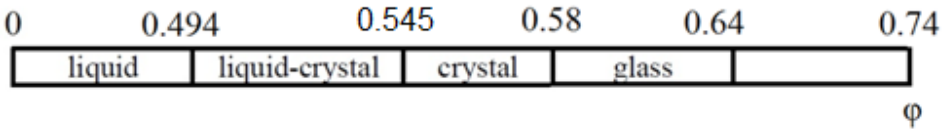

Figure 2.1.2: *phase diagram of hard spheres*

Metastable glasses: Colloidal suspensions are slow to reach equilibrium from a metastable state. The time that particles need in order to reach equilibrium is given as the relaxation time t_B , which is the time it takes for a particle to move a distance equal to it's radius through Brownian motion. The relaxation time depends on the radius of the particle cubed (R^3). However, the hard sphere colloids in disordered suspensions above 58% volume fraction, become tightly trapped or caged, by their neighboring particles and are unable to move enough space for a crystallizing state to exist. Instead of a crystal long-lived amorphous states are obtained that are called colloidal glasses.

2.2 Rheology:

Rheology from Greek ῥέω, "flow" and -λογία, -*logia*, "study of") is the study of the flow of matter. The term rheology was established by Eugene Bingham, a professor at Lafayette College in 1920. The inspiration of the term was due to the phrase of Heraclitus, **«τα *πάντα ρει*»** which means "everything flows". Rheological measurements are applied in substances which have a complex molecular structure, such as suspensions, muds, suspensions, polymers and colloids. Theoretical aspects of rheology are the relation between the internal structure and the flow/deformation behavior of the material.

The disciplines of elasticity and fluid mechanics cannot be described fully from classical theories, while rheology is principally concerned with the extension of these. Materials flow when they are subjected to stress. Different kinds of stresses exist and materials respond to them in different ways. For example there is torsional stress and shear stress. Furthermore, theoretical rheology is primarily concerned with forces associated with flow, external applied stresses and resulting internal strains.

Regarding the Rheological measurements, the aim was to show how the storage modulus G΄ and the loss Modulus G΄΄ develop in relation to varying strain and frequency. The storage modulus G' describes the elastic, whereas the loss modulus G'' describes the viscous properties of the material respectively. The complex modulus G* consists of both moduli with this relationship G*=G'+i*G''. Furthermore, Dynamic time sweeps were measured keeping a constant frequency and strain, in order to collect the Fourier transform signal and Echo peaks.

The applications are vast and some of them are substances which have a complex microstructure, like suspensions, polymers, colloids, bodily fluids (blood) and other biological materials.

Rheometric measurements:

There are two types of rheometers, the ones that create a specific stress field (stress controlled rheometers) or deformation (strain controlled rheometers) to the sample. Both instruments can be operated in steady flow or oscillatory flow, in both shear and extension. The problem when working with commercial rheometers is that experimental data is hard to reproduce, since geometries differ from the simple shear geometry provided. For the solution of this issue, experimental rheologists decided to turn to rotating geometries. Some examples are cone plate and parallel plate geometries. The main difference between the two geometries is that in parallel plates the strain field is not homogenous and the velocity varies, whereas in the cone and plate the strain field is homogenous and the velocity has the same value everywhere. This is an important attribute of the rheometers, since when nonlinear measurements take place the validity of the response relies strongly on the assumption that the whole sample can respond uniformly to applied strain. For linear measurements this assumption is true even when we are using a parallel plate geometry. In our experiments a cone and plate geometry was used, since nonlinear measurements were performed.

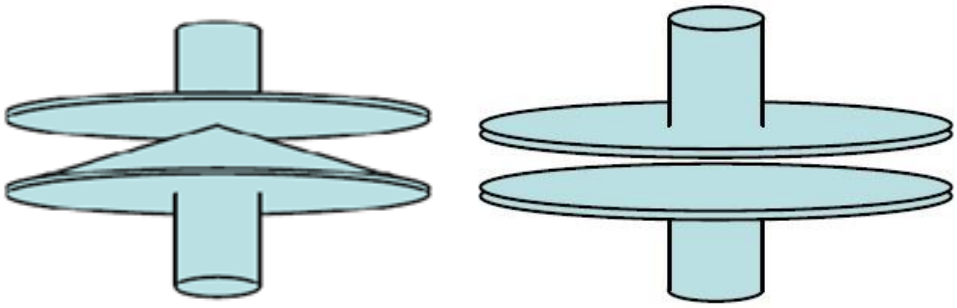

Figure 2.2.1: *Illustration of cone and plate (left) and parallel plate (right) geometries used in experimental rheology.* [17]

Dynamic measurements

Oscillatory shear: a sinusoidal strain with anglular frequency ω is applied to the sample

$$\gamma(t) = \gamma_0 sin(\omega t)$$

This kind of deformations can be achieved in a cone and plate geometry with a rotating bottom-plate about its axis. If the strain amplitude γ_0 is small enough that the fluid structure is not disturbed so much by the effect of deformation, then the stress measured during the oscillatory deformation is controlled by the rates of spontaneous rearrangements.

The viscoelastic response can be explored, with varying frequency on different timescales. If the material is a perfectly elastic solid, then it obeys Hooke's Law

$$\sigma(t) = G\gamma(t) = G\gamma_0 sin(\omega t)$$

Whereas, for a Newtonian liquid the stress will be related to shear rate through Newtons Law:

$$\sigma(t) = \eta \frac{d\gamma(t)}{dt} = \eta\gamma_0 \omega cos(\omega t)$$

The stress in a Newtonian liquid is out of phase with the strain by π/2 since it is expressed as a Cosine, while it still oscillates with the same angular frequency ω.

A small amplitude deformation that is proportional to the amplitude of the applied strain γ_0 produces the shear stress σ(t) and it is itself varying sinusoidally with time.

The total sinusoidally varying stress can be represented as:

$$\sigma(t) = \gamma_0[G'(\omega)\sin(\omega t) + G''(\omega)\cos(\omega t)]$$

Where G´ is the storage modulus and G´´ is the loss modulus. The storage of elastic energy is represented with the storage modulus, while the viscous dissipation of that energy is represented with the loss modulus. When G´ > G´´ the materials has a solid-like behavior, but when G´´ > G´ the material has liquid-like behavior.

Peclet Number

The Peclet number is introduced in order to quantify the effect of shear on a material. By normalizing the Dynamic frequency sweep and Dynamic strain sweep access is gained to the different Peclet regimes available $Pe=\gamma t_B$, where $t_B = \frac{6\pi\eta_S R^3}{K_B T}$ is the Brownian relaxation time, which is the time a particle needs to do a distance equal to it's radius. As noted before there are two rearrangement mechanisms in Colloidal systems under oscillatory shear 1) Brownian motion at low Peclet regime 2) Shear induced collision at high Peclet regime, and both at intermediate Peclet regime. The relaxation time is inherent for the two particle sizes that are being used in our experiments. (t_B=1.1 s for big particles R=358nm, and t_B=0.05 s for small particles R=137nm), thus in order to access different Peclet regimes frequency needs to be altered. For Pe_ω <<1 Brownian motion dominates, for 0,1<Pe_ω<1 both mechanisms are active and for Pe_ω >>1 Shear induced collision dominates. With the small particles (R=137nm) the low and intermediate Peclet regimes are being explored, while with the big particles (R=358nm) the intermediate and high Peclet regimes are being accessed. In the case of oscillatory shear measurements $Pe'=\omega t_B$ is defined, which contemplates to the relevant frequency of oscillatory shear compared to the Brownian time scale. Pe' describes if the frequency is comparable or faster than Brownian motion.

2.4 Rheology of Hard spheres:

Rheological measurements on hard spheres have been done in the past, mostly with polydisperse samples, so that complications due to shear induced crystallization would not occur [7], [8]. With increasing φ, the particles become increasingly crowded by their neighbors, and structural relaxation of the particles slows dramatically, while a liquid undergoes shorter timescales for structural relaxation than a glass because of the particles free motion. As the volume fraction of the glass transition is approached the sample relaxes much more slowly. As a consequence, they can transmit forces like a solid (increased G'). Large-scale collective motion of particles result in structural relaxation, and the range of these events increase closer to the glass transition. In chapter 4 DSS curves are introduced for both particle sizes, where, for comparison purposes the storage and loss moduli, G' and G'', were normalized by thermal energy while on the same time frequency was normalized by the Brownian relaxation time,

($Pe_\omega=\omega t_B$) in figure *4.1.1*. In the glass regime PMMA hard spheres show solid-like response with G'>G'', a weak increase of G' with increasing frequency and a G'' minimum [9], [10].

2.5 Lissajous–Bowditch plots:

The onset of a nonlinear stress response to oscillatory shear can be visualized by Lissajous plots, in which the intracycle stress is shown either as a function of strain or strain rate in order to highlight the the elastic and viscous parts of the system response, respectively. Stress and strain are in phase for elastic materials, where stress (y axis) is maximum when strain (x axis) is maximum also. As a result, this leads into a straight line on this plot, in case of linear elastic materials. On the other hand, they are out of phase ($\pi/2$) for viscous materials (liquids), where maximum stress is obtained when the strain rate is maximum. This behavior leads in a circular Lissajous plot, if the fluid is linear viscous or Newtonian. In the case of a viscoelastic materials, with a phase lag of $0<\delta<\pi/2$, the Lissajous plot is elliptical [13]. All these material behaviors are visualized in figure *2.5.1*. Any deviation from the elliptical shape, indicates the presence of higher harmonic contributions. As the strain is increased, the onset of nonlinearity in the material's response is clear by observation of the distorted Lissajous plots that appear more open. At the same time the elastic stresses progressively deviate from linearity with increasing strain, revealing a rich material response with thinning/hardening contributions depending on the frequency and particle size. The elastic modulus is represented by the tangent slope at zero strain, and the slope of the secant at maximum strain. At maximum strain the secant is not equal to the semimajor axis of the ellipse, except in the case we are studying a purely elastic solid. On the other hand, the slope of the semimajor axis of the ellipse represents the magnitude of the complex modulus [1].

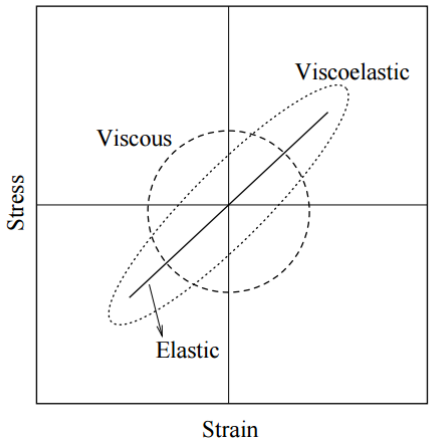

Figure 2.5.1: *Stress versus strain during a cycle for different materials* [13].

2.6 Fourier transform:

The phase difference between strain and various harmonics of stress can be different. As a consequence, amplitude and phase of each harmonic are independent characteristics of the material. The linear regime is confirmed by FT analysis, which shows only a contribution from the fundamental harmonic in the stress response. The non-linearity can be quantified through FT analysis, where there is a strong contribution from higher odd harmonics. It should be noted that even harmonics are virtually zero suggesting the absence of wall slip and shear banding. [12]

2.7 Light scattering Echo:

Rheology can explain the behavior of colloids under shear, yet only simulations can elucidate the physical origin of the system. While light scattering echo can also help in gaining a better understanding of the system experimentally in that sense. Light scattering echo is the combination of rheology and light scattering, aiming in obtaining the diffusion speckle pattern of particles under shear. Echo-DWS [6], [14], [15] is based on light multiply scattered by turbid samples. Upon application of oscillatory shear changes in the time autocorrelation function of the scattered light are exploited to determine shear-induce particle dynamics with repeating echoes that are visible on the system period multiples (mT)[16]. The correlation function $\sqrt{g^{(2)}-1} = \exp(-\frac{1}{6}nk^2\langle\Delta r^2\rangle)$ where n is the number of times the beam is scattered by the sample (we assume two here) and $k = \frac{2\pi}{\lambda}$ the waveguide, always start from value 1 (initial state) where 100% correlation is attained. If the system responds elastically, the particles return to their initial position after an integer

time of oscillation periods hence the correlation function returns to 1. On the other hand through shear plastic rearrangements are introduced to the system resulting in values of the correlation function less than 1. There are two kinds of mechanisms that can introduce rearrangements to the particles: 1) Brownian Motion 2) Shear induced Collision. In chapter 2 the idea of Peclet number was introduced, in order to distinguish these two yielding mechanisms. To recap, In the region of low Peclet: (Pe<<1) Brownian motion dominates, whereas in the regime of high Peclet: (Pe>1) shear collision dominates. However, on intermediate Peclet (0,1<Pe<1) both mechanisms co-exist. In addition the correlation function becomes: $\sqrt{g^{(2)}-1} = \exp(-\frac{1}{6}nk^2[\langle \Delta r^2\rangle_B + \langle \Delta r^2\rangle_S])$, where $\langle \Delta r^2\rangle_B$ are the rearrangements induced by Brownian motion and $\langle \Delta r^2\rangle_S$ the rearrangements induced by shear.

Small (R=137nm) and big particles(R=358nm) are utilized in our experiments, so that access is gained to all Peclet regimes, since relaxation time t_B cannot be altered. Echoes are visible with up to 30% strain (2Hz frequency in big particles R=358nm).The relative first echo decreases with increasing strain amplitude and after approximately 2-3% the non-linear behavior of our system can be clearly shown, as well as from FT analysis. LS Echo gives us a more convincing explanation of the physical picture of colloidal particles, while on shear. Brownian motion introduces less abrupt rearrangements compared to shear induced collision.

By normalizing the echo peak height with the first strain we measured (0.5 or 1 %), all the Brownian motion contributions were successfully extracted and therefore it was clear how the mechanism of shear collision is related to plastic rearrangements. The short-Brownian diffusion was visible in smaller timescales, through the fast drop of the correlation function. Also the inverse of half of the half width of the first echo peak was calculated, which shows an increasing trend with increasing frequency and a decreasing trend with increasing strain (peaks get narrower with increasing strain).

Chapter 3: Experimental techniques and details:

3.1 Samples:

Two kinds of hard sphere particles were used, small (asm340, R=137nm) and big (asm454, R=358nm). These hard sphere particles consist of polymehtylmethacrylate (PMMA) cores that are being sterically stabilized by thin (10nm) chemically grafted polymeric layers of poly-12-hydroxystearic acid (PHSA) chains. The particles have polydispersity of 12% in order to avoid crystallization by shear. The solvent we used is a mixture of bromonapthalene and octadecene (n=1.48) in order to avoid evaporation and to approximately match the refractive index of the colloidal particles (n=1.497). The refractive index of the solvent and the colloids did not entirely match, and as a result the colloidal suspension was turbid and not transparent.

Solvents	Refractive index	Boiling point
Bromonapthalene	1.6494	280 C^o
Octadecene	1.4441	317 C^o

***Table**: Bromonapthalene and octadecene solvents properties*

3.2 sample preparation:

Before preparing the specific volume fractions used, the cleaning process was followed. Firstly, the mixture of solvents are being prepared and then it is added to the colloidal powder in order to create the suspension. Secondly, the suspension is mixed in the vortex and then it is being centrifuged leading to phase separation. Ultimately, the excess solvent is being thrown away, and the whole process is repeated seven times. After the cleaning process, sample dilution followed until the desirable volume fraction was reached: 0.61 and 0.63 for small particles (R=137nm) and 0.61 for big particles (R=358nm).

3.3 Rheometer specification:

An ARES (TA) strain controlled rheometer was used for all measurements. The rheometer's torque range is 0.004-10 $gr \cdot cm$ with the first transduced and 0.04-100$gr \cdot cm$ with the second [14]. Moreover, for our experiment, it was decided to use a homemade cone and plate geometry (Echocone: cone angle=0.04 rad, diameter=40 mm), where the plate is made of glass since it was used for light scattering experiments (LS Echo). A steel spherical solvent trap was used to ensure minimum solvent evaporation during the experiment. In order to ensure reproducibility of measurements, a constant temperature of 20 ℃ was kept

3.4 Rheological measurements and experimental protocol:

An experimental protocol was followed with regard to data validity. Before conducting any measurements a dynamic strain sweep with decreasing strain was performed in the range of 100%-0.5% (Rejuvenation) thus destroying (erasing) any structural memory that the system could have due to stress from loading the sample or from previous experiments. Between the rejuvenation and each measurement a constant waiting time of five minutes was kept. Furthermore, the measurements performed were:

1) Dynamic frequency sweep tests (DFS), where the strain is constant in the linear regime (γ_o =1%) and the measurement of G' and G'' takes place.

2) Dynamic strain sweeps at frequencies of 0.2-2 Hz measuring G' and G'' with varying strain, while the frequency is constant.

3) Dynamic time sweeps (DTS), where G' and G'' is being measured at a constant strain and frequency.

3.5 Echo configuration: An air cooled tube of He-Ne laser of wave-length ($\boldsymbol{\lambda = 633\ nm}$) that is operating at 25mW was used, in order to illuminate the sample. Crossed polarizers are used, so that the incident beam will be eliminated, when measuring the correlation function, thus taking only the scattering beam contribution of the colloidal particles into account. When light is scattered from the sample backscattering occurs and it is captured by the detector which is located above. After that the photomultiplier, multiplies the scattered light intensity and as a consequence individual photons can be detected even when the incident flux of light is very low. Then the light patterns are being converted into electric signal, which are being correlated by the correlator.

The most important configuration options are: The **echo width**, which actually changes the time space where the echo peaks appear. The **sample time**, which is the average time of photons that are being captured, the **Echo points**, where the number of points in every echo is specified. The only restriction is the channel capacity that is frankly the available data slots which can be monitored, so that more data points go into a specific region of the echo. Another important factor that we can manipulate is the **correction factor**, which gives us the opportunity to fix the error induced by the correlator clock in long times of correlation, thus fixing the last peaks position. Another configuration option is the **ratio of points around base line to initial decay**. For bigger ratio values, more points are acquired around the base of the echoes as opposed to the initial decay of the correlation function due to short-time Brownian motion.

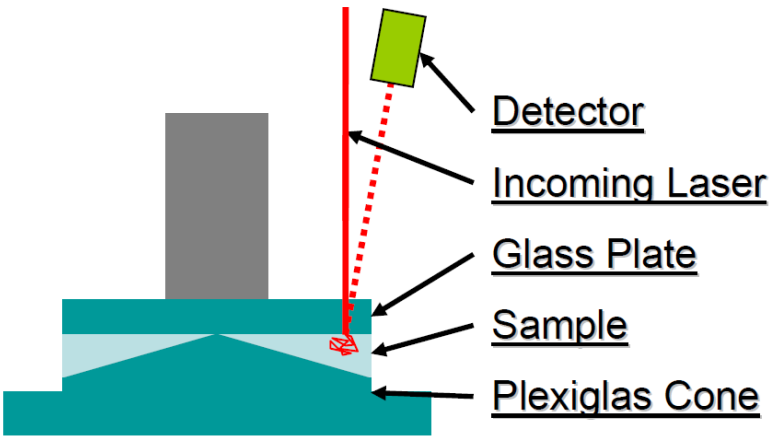

Figure 3.5.1: LS *Echo setup schematic* [17].

Chapter 4: Results and Discussion

4.1 Rheology of hard sphere glasses:

Linear Rheology: In general, Dynamic frequency sweep tests were performed for determining the storage (G') and loss (G'') modulus as seen in figure *4.1.1*. The frequency sweeps were performed with 1% strain for all the samples, while the volume fraction is almost matched. Waiting time before performing measurements is $6000t_B$ for small particles and 273 $t_{B\ for}$ big particles. In order to determine the linear regime, Dynamic strain sweep measurements were performed for φ=0.61 volume fraction. In figures *4.1.2* and *4.1.3* both particles show an increased storage modulus G' with increasing frequency, while the novel loss modulus minimum which is characteristic of colloidal gels and glasses is observed. The characteristic time for a particle to explore it's cage is related to the minimum of G''. In small particles G' and G'' values are much higher than in big particles, because there is a direct proportionality to the thermal energyK_BT.

Non-Linear Rheology: Two different frequencies were applied 2Hz and 0.2Hz. For the small particles (R=137nm) the linear regime extends from 0.5% to 1.34% strain as seen in figure *4.1.2*, wherein for the big particles(R=358nm) in figure *4.1.3* the linear regime extends from 0.5% to 1% strain. Additionally in both cases shear thinning behavior is observed, where G' decreases and G'' increases at the same time showing the material's pronounced viscous behavior.

For the small particles and 0.2Hz frequency the G'' double peak is observed, as a result of the two rearrangement mechanisms found in colloidal system under oscillatory shear 1) Brownian motion assisted cage escape on low Peclet and 2) Shear induced collision at high Peclet . The two peaks signify maximum energy dissipation during the two yielding mechanisms, which is attributed to cage breaking from thermal motion and through particle collisions respectively [3]. Moreover, big particles show an anisotropic structure under, that exhibits an interesting hysteresis under strain reversal. With this kind of structural "memory", a characteristic stress drop is observed after strain reversal through The Lissajous plots, shown in chapter 4.2.

Dynamic Frequency sweep

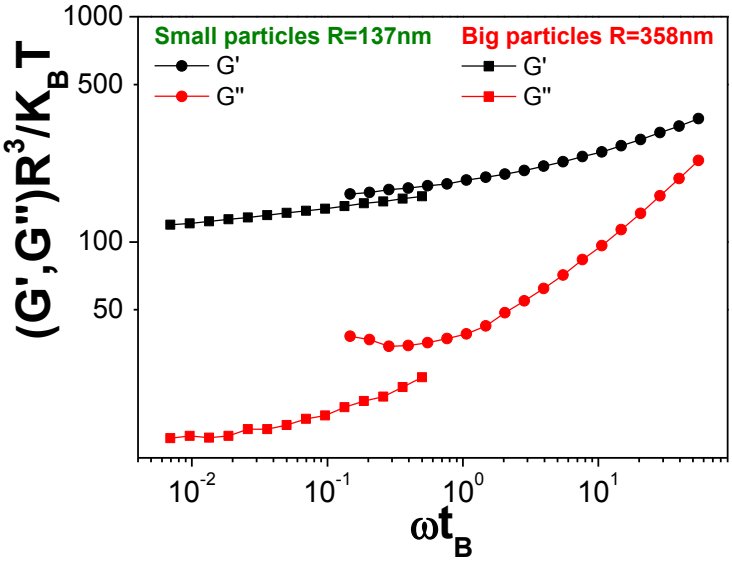

Figure 4.1.1: *Normalized Dynamic frequency sweep for PMMA Colloidal hard spheres of Radius R=137nm* and R=358nm.

Big particles (R=358nm)

Dynamic Strain Sweep

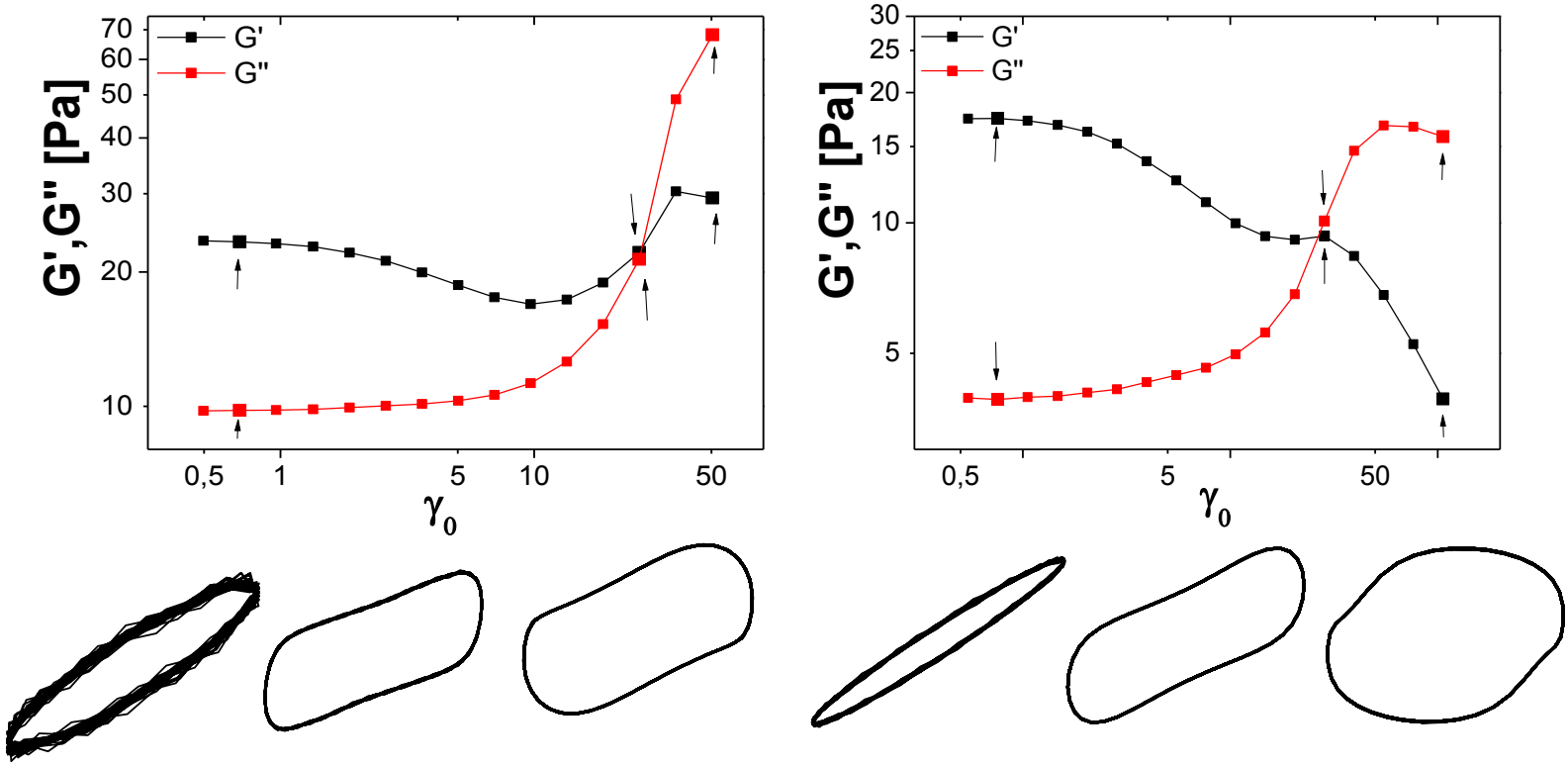

Figure 4.1.2: *Dynamic strain sweep with 2Hz frequency (left),0,2Hz (right) for PMMA Colloidal hard spheres of Radius R=358nm.*

Small particles (R=137nm)

Dynamic strain sweep

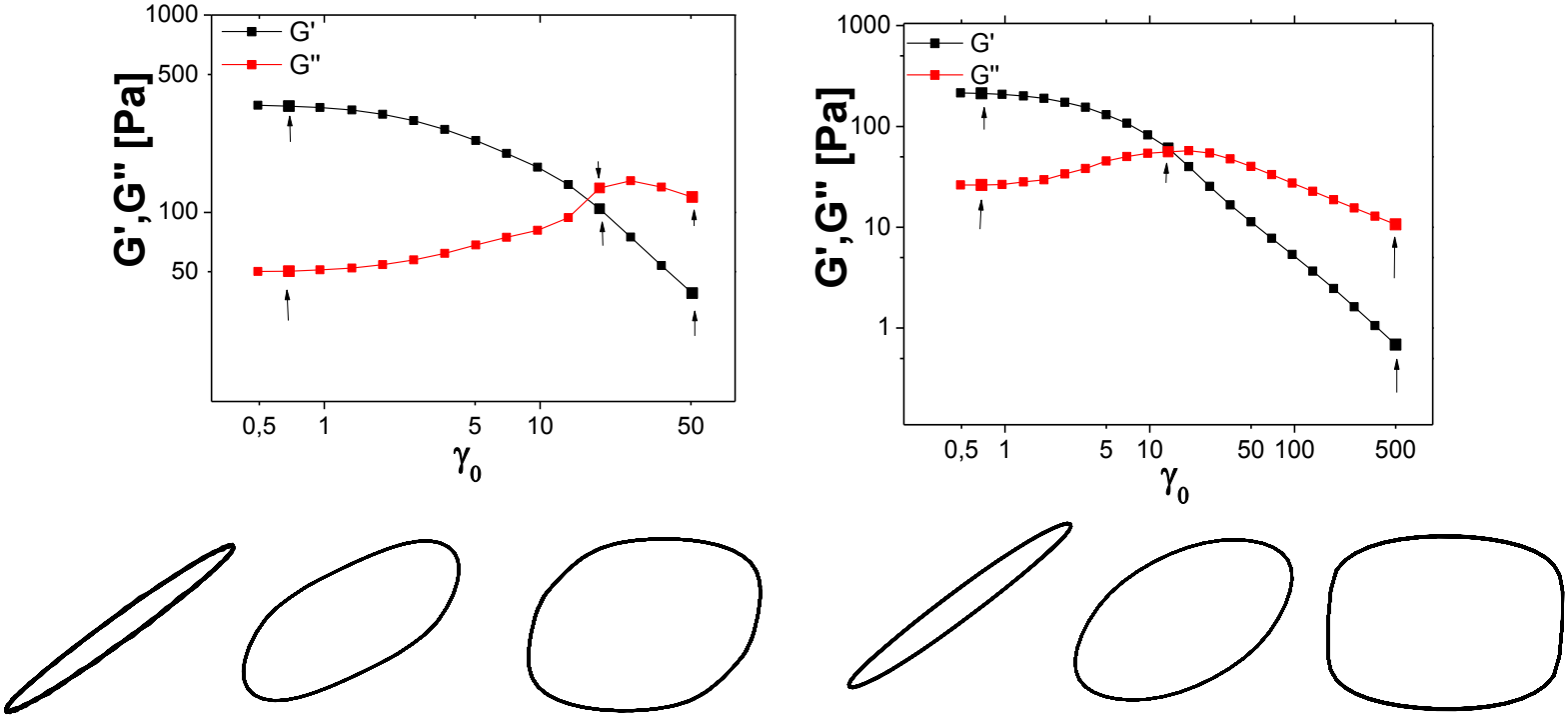

Figure 4.1.3: *Dynamic strain sweep with 2Hz frequency (left),0,2Hz (right) for PMMA Colloidal hard spheres of Radius R=137nm.*

4.2 Lissajous-Bowdich Plots:

Big particles (R=358nm)

2 Hz

0,2 Hz

0,05 Hz

0,5% **1%** **5%** **10%** **15%** **20%** **25%** **30%** **35%** **40%**

0,2 Hz

0,05 Hz

45% **50%** **60%** **70%** **90%** **100%**

Small particles(R=137nm)

2 Hz

0,2 Hz

0,05 Hz

0,5% **1%** **5%** **10%** **15%** **20%** **25%** **30%**

2 Hz

0,2 Hz

35% **40%** **45%** **50%** **60%** **70%** **90%**

100% **200%** **300%** **400%** **500%**

Big particles (R=358nm) can reveal the transition from the low peclet rectangular shape Lissajous plot that shows both elastic and plastic responses, until the high Peclet regime to the ellipsoid with a double concave distortion shape that is attributed to the reduction of stress, which is also shown with Fourier analysis on the next chapter.

Progressively larger intracycle non-linearities accompany the non-linear response, as indicated both by the Lissajous plots here and Fourier transform in the chapter 4.3. Moreover, small particles (R=137nm) show a transition on Lissajous plots from a linear visco-elastic behavior (regular elliptical shape) to low strains, to a distorted parallelogram pattern which indicates the elastic to plastic response.[3]

4.3 Fourier transform:

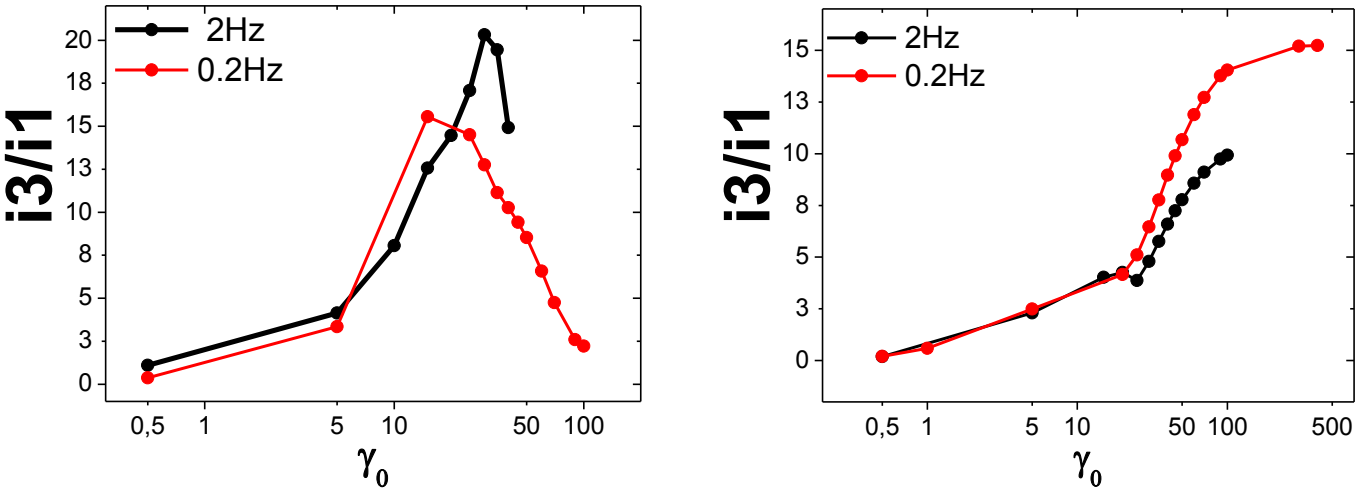

Figure 4.3.1: *Third harmonic response of PMMA colloidal spheres of 0.61 volume fraction versus strain amplitude for all frequencies applied and radius of R=358nm (left) and for R=137nm (right).*

FT analysis is shown in figure 4.3.1 for 61% volume fraction in both particle sizes, where the higher harmonic contributions relative to the fundamental I_3/I_1 , are plotted versus the applied strain for both particle sizes. In the linear regime at 0.5% only the fundamental harmonic is contributing to the stress response. At higher strains the higher odd harmonic contributions become significant, due to the increased stress non linearity. It is clear that in both cases, lower frequencies have a larger amplitude of non-linearity, which starts around γo=2-3% for both particle sizes. Additionally, a

more gradual increase is observed for the small particles, while for the big particles it is abrupt on γ_o=15% for both frequencies. With further increase of γo a drop is witnessed for the big particles at 30% for 2Hz frequency and at 25% for 0.2Hz until 50% and 100% respectively, in contrast with the small particles where an increasing trend is still contemplated until 100% for 2Hz frequency and 500% for 0.2Hz. Clearly for the big particles a more anisotropic particle cage is formed due to fewer particle collisions, thus allowing flow with less stress compared to the small particles where Brownian motion relaxes shear-induced structural anisotropy more efficiently, leading to an increasing stress response.[3]

4.4 Light scattering echo:

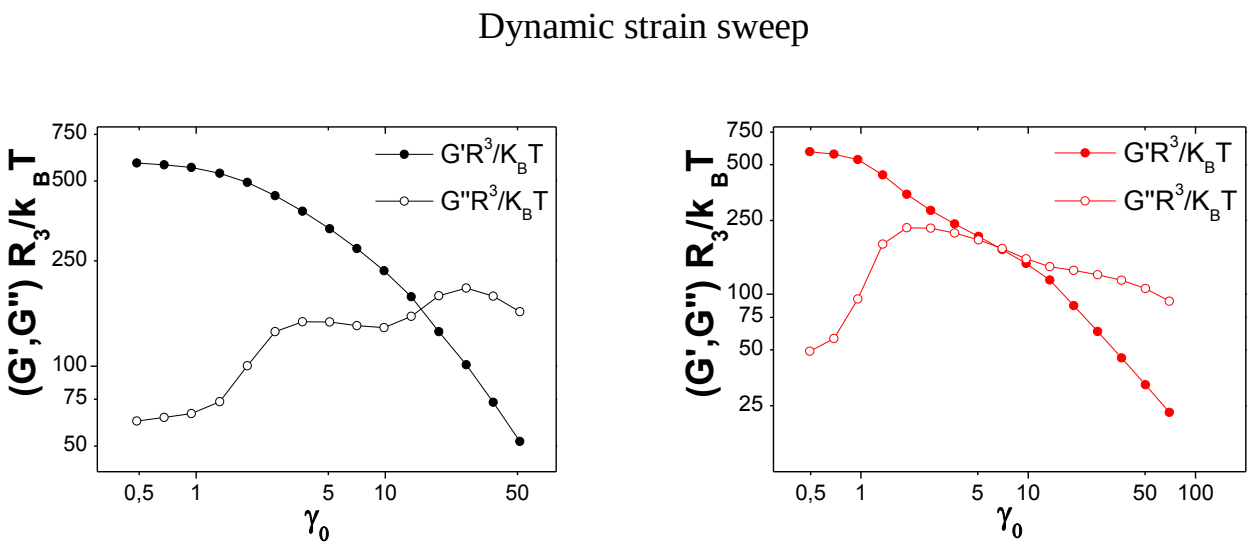

Figure 4.4a: *Normalized Dynamic strain sweep for 2Hz and 0.5Hz frequency for PMMA Colloidal hard spheres of Radius R=137nm and volume fraction φ=0.63*

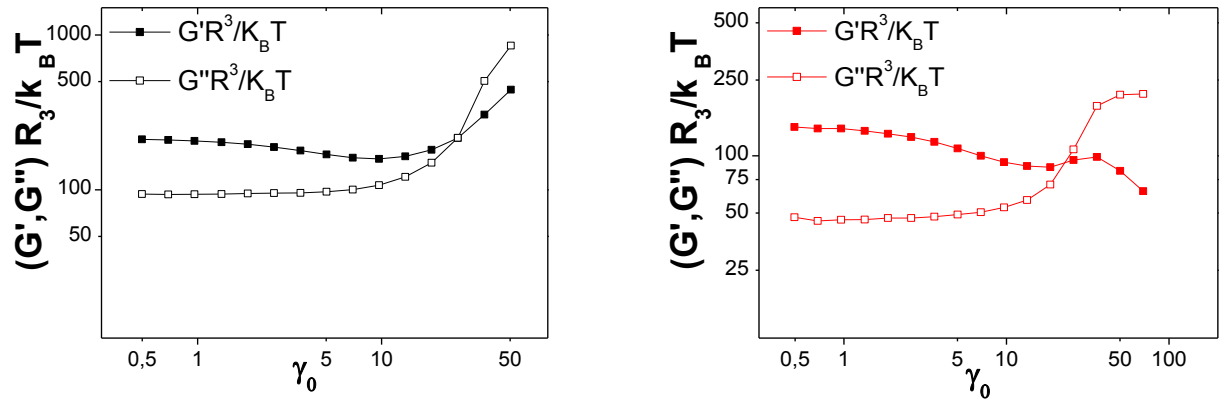

Figure 4.4b: *Normalized Dynamic strain sweep for 2Hz and 0.5Hz frequency for PMMA Colloidal hard spheres of Radius R=358nm and volume fraction φ=0.61*

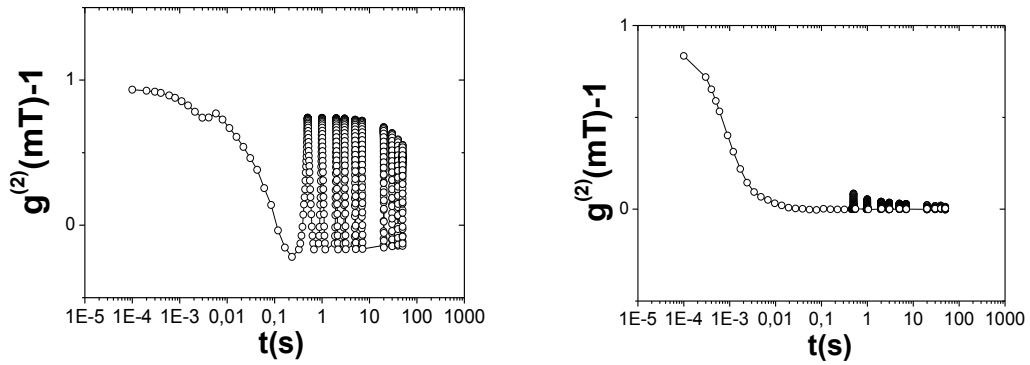

Figure 4.4.0: *Time autocorrelation function of a linear (2Hz 0.5% strain) {left} and a non-linear (2Hz 15% strain) {right} measurement for small particles (R=137nm) of 61% volume fraction.*

The time autocorrelation function exhibits echoes in multiples of the oscillation period, as noted in chapter 2.7 in order to monitor the elastic and plastic behavior of the colloidal particles. The volume fraction is set to 61%.On the left of figure *4.4.0* for frequency of 2Hz and 0.5% strain the system responds elastically since even in long timescales, it exhibits the same echoes indicating no structural changes, almost like a solid material. Wherein for 2Hz and 15% strain the non-linear behavior is clear, due to the almost complete disappearance of the echoes in long timescales indicating that the material is starting to respond like a liquid. Moreover, it has to be noted that even the first echo peak is decorralated in the latter case, showing that irreversible rearrangements occur even at short timescales when the material is a fluid.

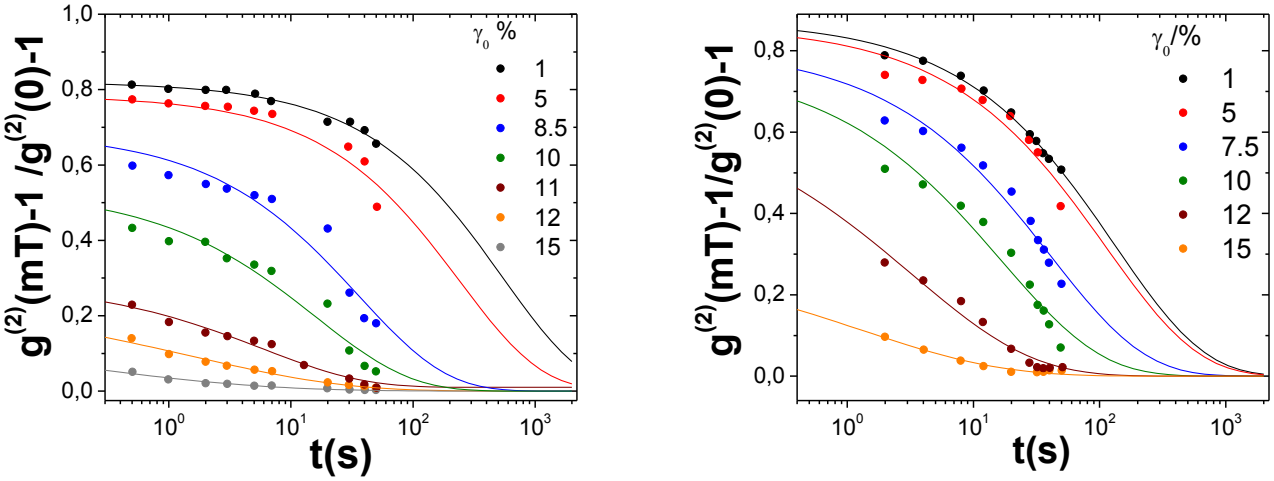

Figure 4.4.1: *Light scattering echo peak height fitted with an exponential decay function for all strains applied with frequency of 2Hz (left) and 0.5Hz(right)on PMMA Colloidal hard spheres of Radius R=137nm and volume fraction of φ=0.63.*

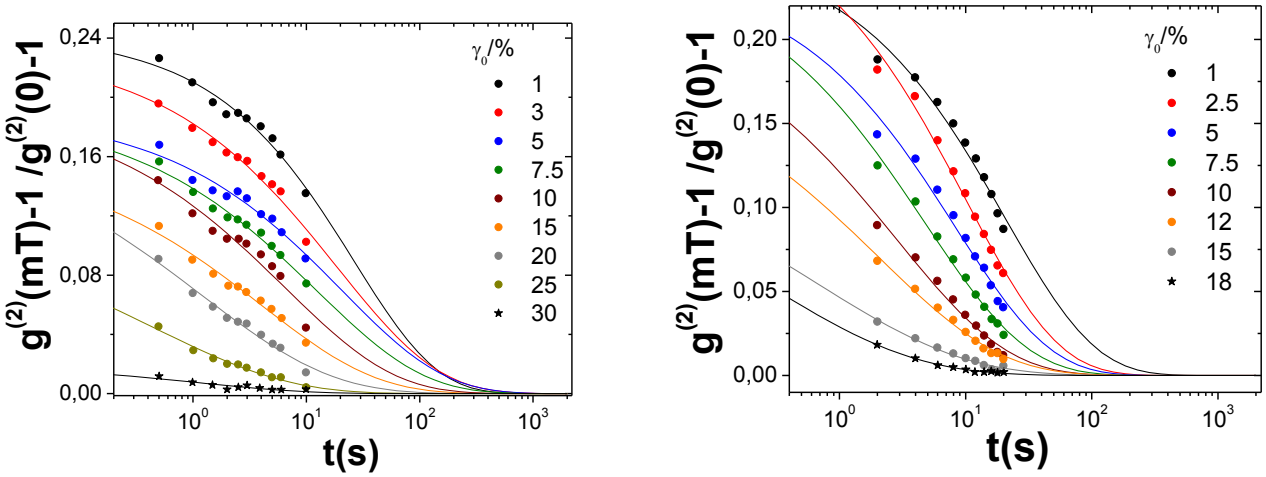

Figure 4.4.2: *Light scattering echo peak height fitted with an exponential decay function for all strains applied with frequency of 2Hz (left) and 0.5Hz(right)on PMMA Colloidal hard spheres of Radius R=358nm and volume fraction of φ=0.61.*

The stretched exponential was fitted for both systems: $y = A * e^{\left(-\frac{x}{t_\beta}\right)^\beta} + C$, where A is the amplitude t_β is the relaxation time, β is the stretching exponent ($0 \leq \beta \leq 1$) and C is the offset. In the linear regime, for both systems the height of the first echo is virtually independent of the strain amplitude (γ_o =1%). In figure *4.4.1* for small particles, a higher timescale was available until 50 seconds, however in figure *4.4.2* for big particles a timescale of only 10 seconds was reached for 2Hz frequency and 20 seconds for 0.5Hz since echo peaks disappeared at larger times. Above the amplitude of 1% in the Non-linear regime, the echo height significantly decreases with γ_o ,

following a stretched exponential decrease with a dramatic change around γ_o=8.5% and γ_o=7.5% in 2Hz and 0.5Hz frequency respectively for the small Particles in figure *4.4.1* and around γ_o=5% in 2Hz and 0.5Hz in figure *4.4.2* for the big particles. The peaks completely disappear at 15% for the small particles in both frequencies and for the big particles at 30% and 18% for 2Hz and 0.5Hz respectively.

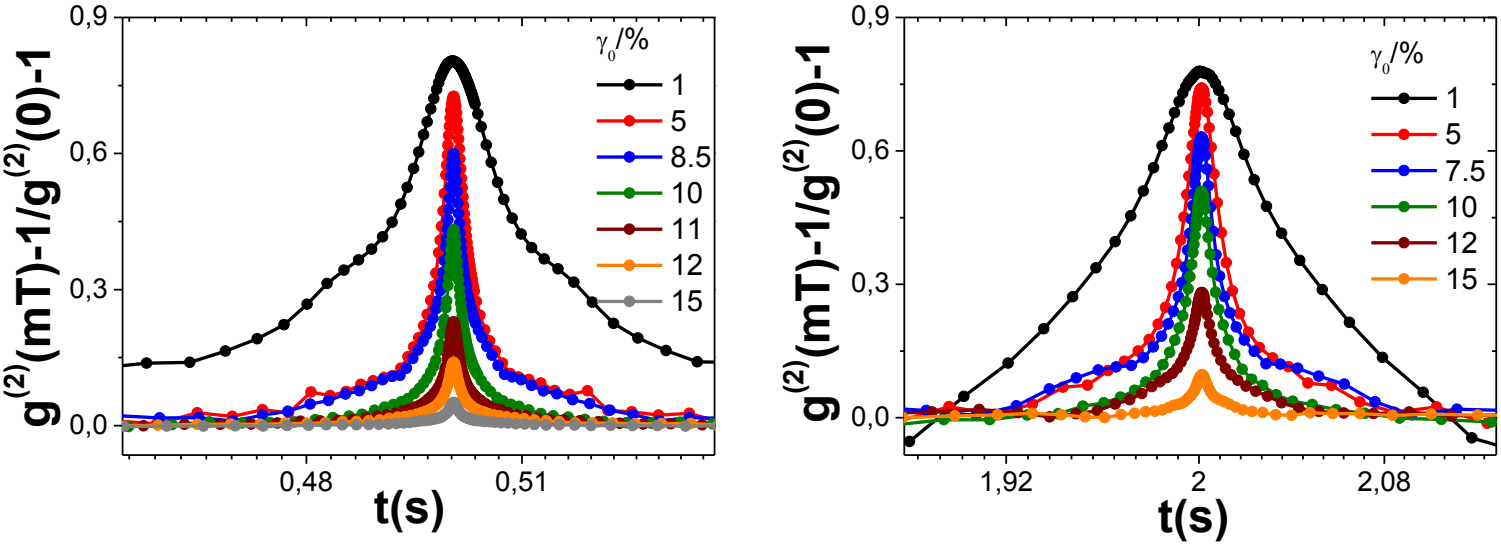

Figure 4.4.3: *First echo for all strains applied with frequency of 2Hz(left) and 0.5Hz (right) on PMMA Colloidal hard spheres of Radius R=137nm and volume fraction φ=0.63.*

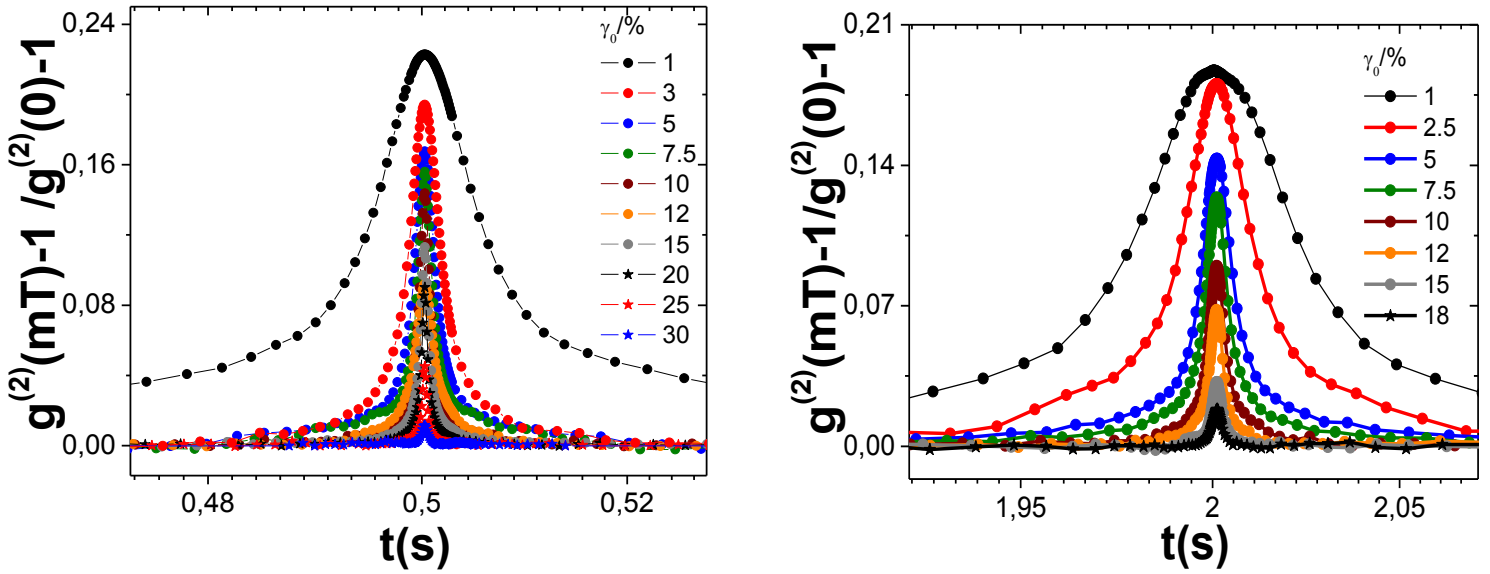

Figure 4.4.4: *First echo for all strains applied with frequency of 2Hz(left) and 0.5Hz (right) on PMMA Colloidal hard spheres of Radius R=358nm and volume fraction φ=0.61.*

The amplitude of the first echo decreases rapidly with increasing strain as was also observed in figures *4.4.1 and 4.4.2*, showing the shear induced irreversible particle rearrangements that are gradually increasing around γ_o=8.5% and γ_o=7.5% in figure

4.4.3 for 2Hz and 0.5Hz frequency respectively for the small particles (R=137nm) and around γ_o=5% in figure *4.4.3* 2Hz and 0.5Hz for the big particles (R=358nm).Also it is noted that, the echo width is decreasing with increasing strain showing the pronounced viscous behavior due to the fact that echo width is proportional to the shear relaxation time.

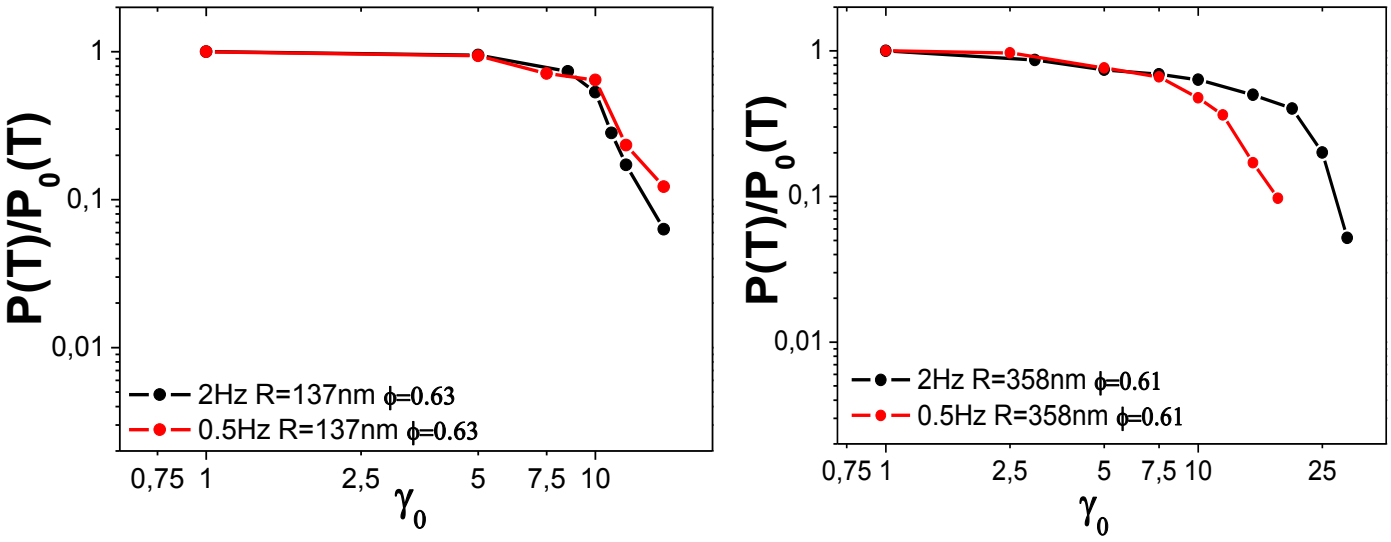

Figure 4.4.5: *Shear induced decay of relative first echo of all strains applied of frequencies 2Hz and 0,5Hz on PMMA Colloidal hard spheres of Radius R=137nm (left) and R=358nm (right).*

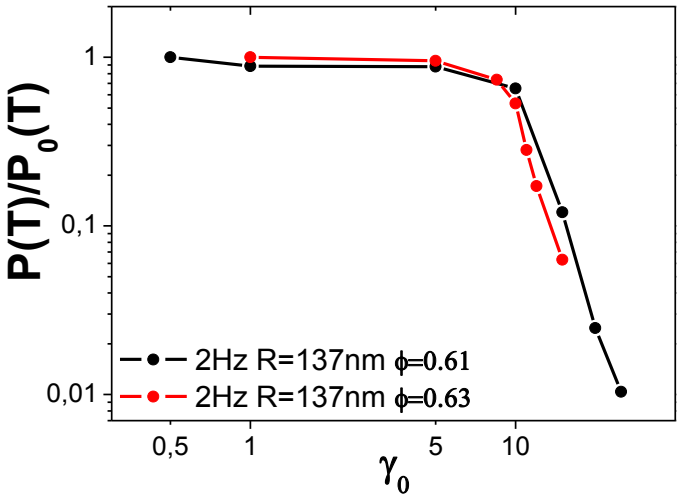

Figure 4.4.6: *Shear induced decay of relative first echo of all strains applied for all volume fractions on PMMA Colloidal hard spheres of radius R=137nm*

From the correlation function, one can extract all the Brownian motion contributions, with $\frac{P(T)}{P_0(T)} = \frac{P(T)}{\lim_{\gamma_0 \to 0} P(T)} \approx \exp\left[-\frac{1}{6}Nk^2\langle \Delta r^2(t)\rangle_S\right]$ normalizing with strain in the limit of 0% strain (0.5% for small particles 61% volume fraction, 1% for all the rest). In figure *4.4.6* for both volume fractions of small particles (R=137nm), shear is starting to affect around γ_o= 10-11% for 2Hz and 0.5Hz frequency where an abrupt drop is observed, while on 2Hz and 0.5Hz for the big particles in figure *4.4.5* it starts around γ_o= 7.5%. Furthermore, at γ_o= 15% for small particles and γ_o= 30% for big particles, an abrupt drop is observed in $\frac{P(T)}{P_0(T)}$ and the echo peaks completely disappear since the material becomes a fluid.

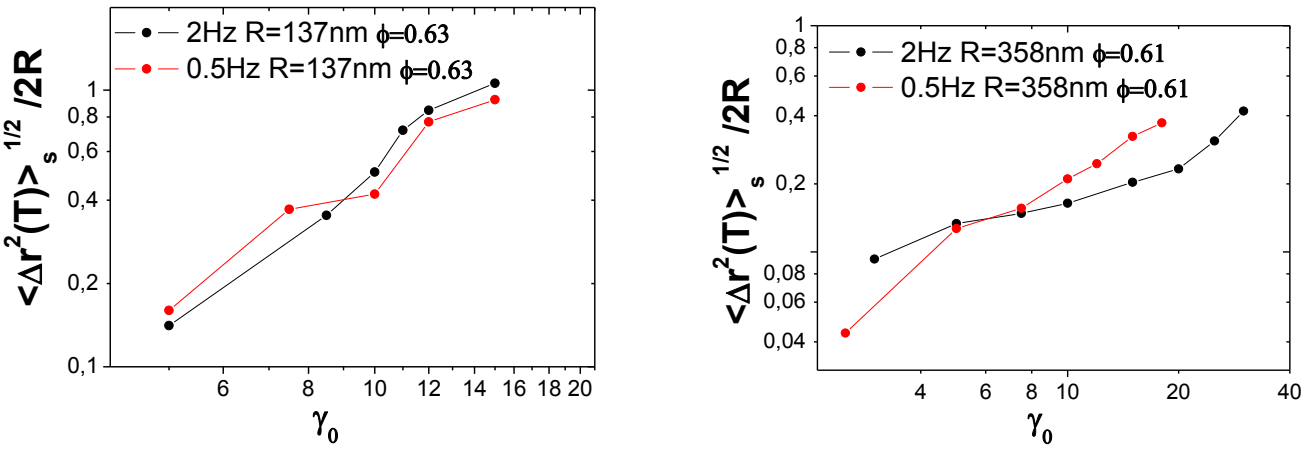

Figure 4.4.7: *Square root of the shear induced mean square displacement as a function of strain amplitude for frequencies 2Hz and 0,5Hz on PMMA Colloidal hard spheres of Radius R=137nm (left) and R=358nm (right).*

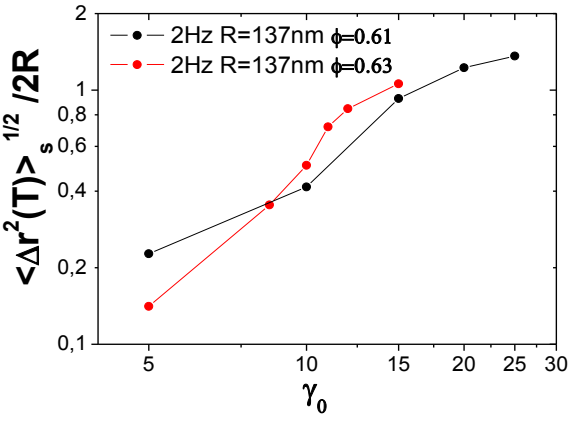

Figure 4.4.8: *Square root of the shear induced mean square displacements normalized to the particle diameter as a function of strain amplitude for all volume fractions on PMMA Colloidal hard spheres of radius R=137nm.*

In addition to the shear induced decay of the relative first echo, the particle mean square displacement was calculated as well. By using the physical logarithm on $\frac{P(T)}{P_0(T)}$ we obtain $\ln\left(\frac{P(T)}{P_0(T)}\right) \approx \ln\left(\exp\left[-\frac{1}{6}Nk^2\langle\Delta r^2(t)\rangle_S\right]\right)$ leading to $\ln\left(\frac{P(T)}{P_0(T)}\right) \approx \left[-\frac{1}{6}Nk^2\langle\Delta r^2(t)\rangle_S\right]$. Finally, it leads to $\langle\Delta r^2(t)\rangle_S = \frac{\ln\left(\frac{P(T)}{P_0(T)}\right)}{-\frac{1}{6}Nk^2}$. The particle mean square displacement directly follows the material microscopic structural changes induced by shear in order to get a deeper understanding of this mechanism, In other words these rearrangements are directly linked to the decorrelation of the echo peaks. Contrary to what was observed on the shear induced decay of the relative first echo in figures *4.4.5* and *4.4.6* , for the big particles in figure *4.4.7* lower frequencies induce larger rearrangements for γ_o more than 4%. Also, for the small particles in the same figure when γ_o is up to 8% similar behavior is contemplated. However, at higher γ_o rearrangements for 2Hz frequency become larger than those for 0.5Hz. In contrast to what was observed for the volume fraction dependence of small particles in figure *4.4.8*, with the exception of γo =5% larger particle rearrangements are induced for higher volume fractions.

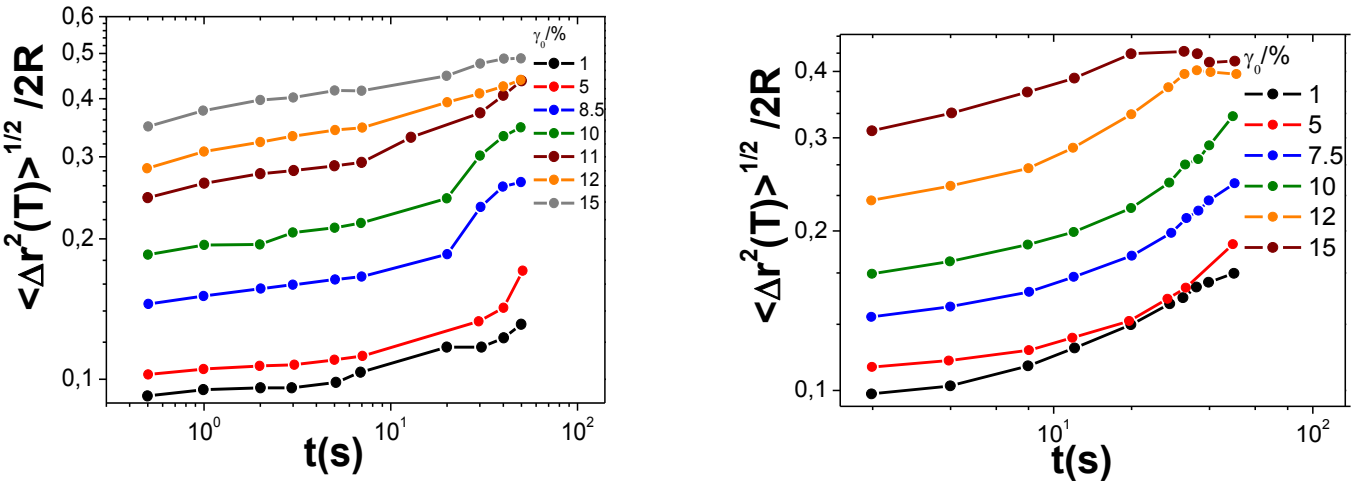

Figure 4.4.9: *Square root of the mean square displacements normalized to the particle diameter as a function of strain amplitude for all volume fractions on PMMA Colloidal hard spheres of radius R=137nm.*

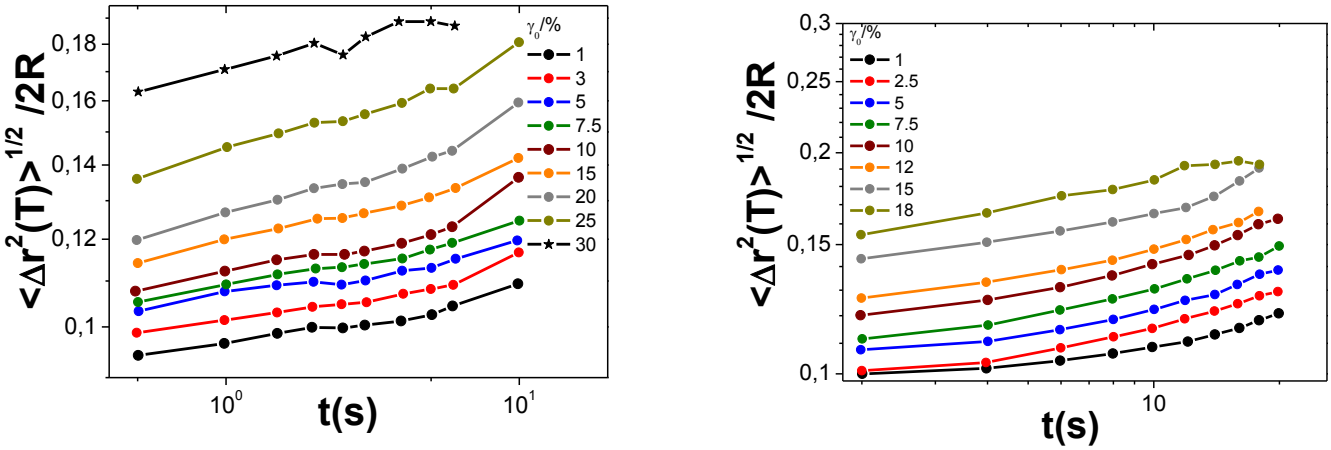

Figure 4.4.10: *Square root of the shear induced mean square displacements normalized to the particle diameter as a function of strain amplitude for all volume fractions on PMMA Colloidal hard spheres of radius R=137nm.*

This mean square displacement consists of both Brownian motion and shear in contrast with the one plotted in figures 4.4.7 and *4.4.8.* where only the shear mechanism is contemplated.

Generally, the mean square displacement increases with increasing γ_o and time as seen in figures *4.4.9* and *4.4.10*. Additionally, a gradual increase is observed around 10 seconds for both particle sizes and a more abrupt around 30 seconds for the small particles while for the big this occurs at 10 seconds. Furthermore, for the small particles a larger mean square displacement is observed showing that more irreversible rearrangements take place compared to the big particles as seen in in figures *4.4.9* and *4.4.10*.

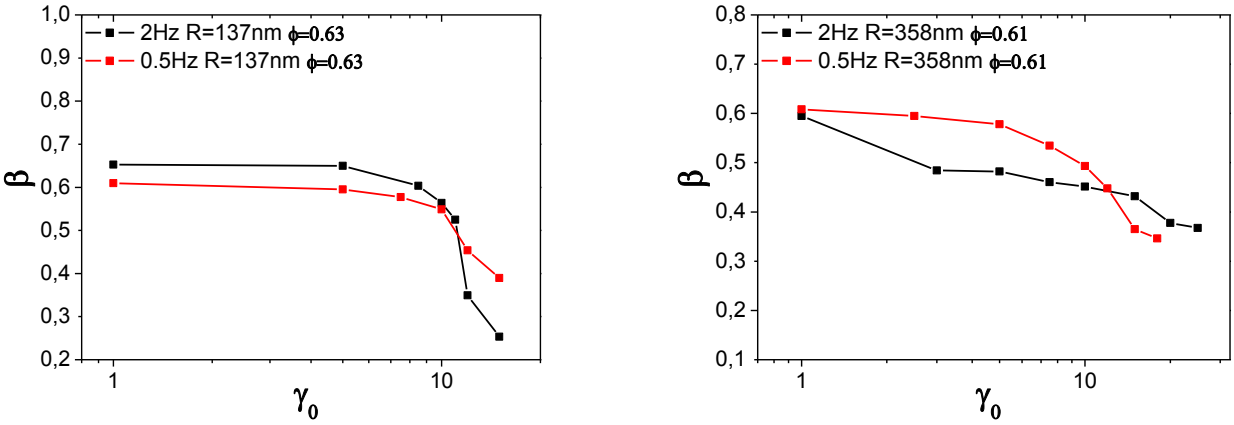

Figure 4.4.11: *Beta exponent as calculated from fitting the stretched exponential ($0 \leq \beta \leq 1$) for small particles (R=137nm) for frequencies of 2Hz and 0.5Hz respectively (left), and for big particles (R=358nm) for frequencies of 2Hz and 0.5Hz (right).*

The stretching exponent β is dimensionless and plays the role of a non-equilibrium scaling exponent with values ranging from 0,6 to 0,25 as seen in figure 4.4.11. For the small particles (R=137nm) and both frequencies there is a decreasing trend with increasing γ_o until the minimum at γ_o=15%, with the values of beta being somewhat larger for 2Hz. The same applies for the big particles (R=358nm) for 2Hz frequency a decrease is contemplated until γ_o=30%. Furthermore, for 0.5Hz an increasing trend is observed until γ_o=18% with values of beta exponent slightly larger than those for 2Hz. The drop of beta with increasing strain amplitude indicates a broader spectrum of relaxation times in both systems.

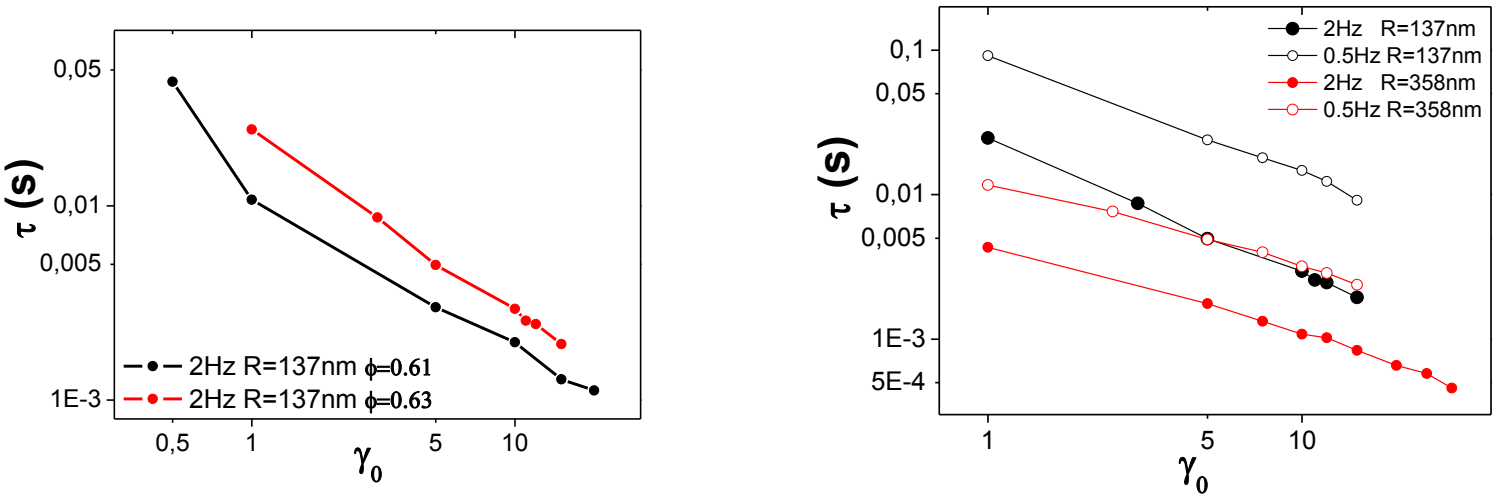

Figure 4.4.12: *Relaxation time through shear of PMMA hard spheres of radius R=137nm and different volume fractions (left) and for radius R=358nm and volume fraction φ=0.61, R=137nm and volume fraction φ=0.63 (right).*

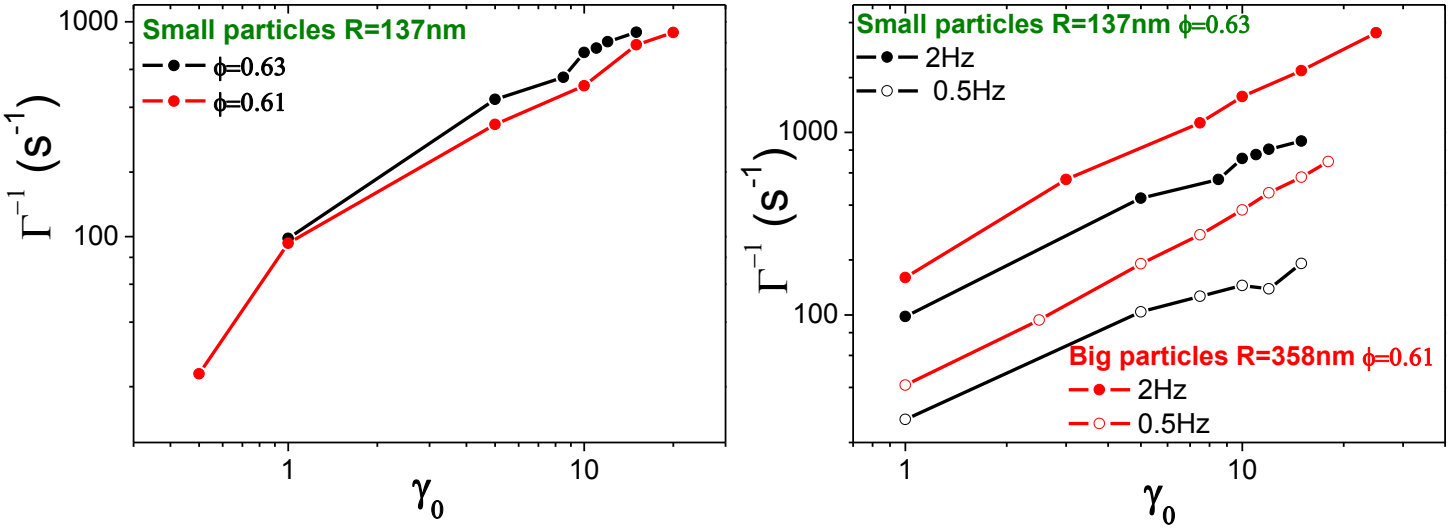

Figure 4.4.13: *Inverse relaxation time of PMMA hard spheres of radius R=137nm and different volume fractions (left) and for radius R=358nm and volume fraction φ=0.61, R=137nm and volume fraction φ=0.63 (right).*

Big particles relax faster than small particles as observed in figure *4.4.12*, where for the same frequency the time scales are smaller. In the same figure, it is clear that the big particles show the same behavior for 0.5Hz as the small particles for 2Hz which indicates that they are in the same Peclet regime. Admittedly, with increasing frequency both systems relax faster due to shear. Moreover, in figure *4.4.12* the lower volume fraction for the small particles relaxes faster than the higher one in agreement

with what was observed by the shear induced decay of the relative first echo in figure *4.4.6*. Finally, concerning the inverse of the half width, which is the actually the inverse of the relaxation time, the desired linear behavior is observed in figure *4.4.13* indicating that there was no wall slip or shear banding in our experiments.

Comparative plots

Size dependence:

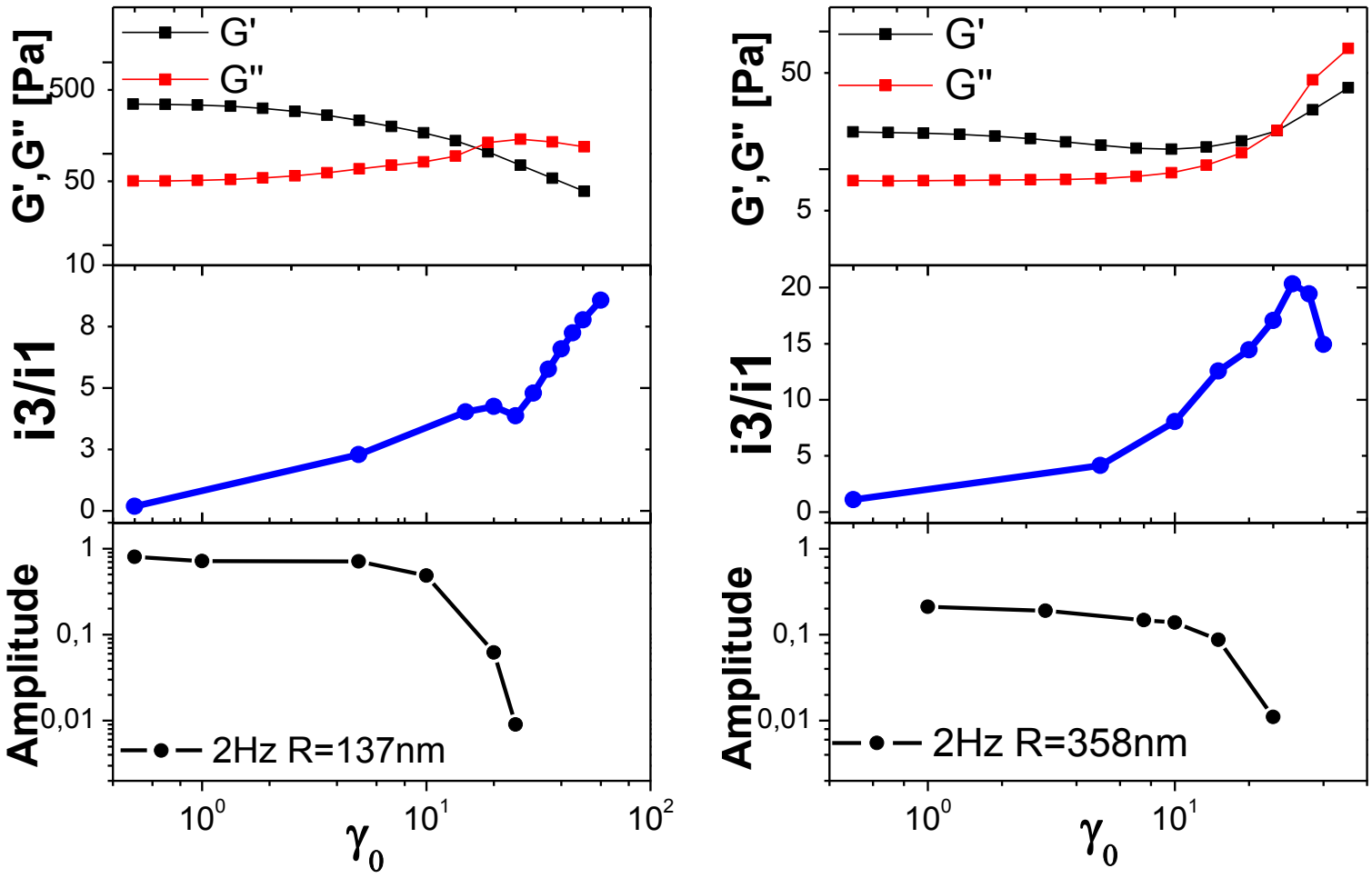

Figure 4.4.14: *Comparison of the elastic G' and viscous G'' modulus, with the third harmonic response and echo amplitude decay for small particles (R=137nm) φ=0.61 with 2Hz frequency (left) and for big particles (R=358nm) φ=0.61 with 2Hz frequency (right).*

With figure *4.4.14* the size dependence comparison is accomplished. For the small particles, G’ is decreasing with increasing strain while G’’ is increasing, starting from low values for the third harmonic showing that only the fundamental harmonic is present while the echo amplitude has not yet decorralated revealing a solid response. The same behavior is contemplated for the big particles also. In addition, for both cases the third harmonic increases with increasing strain, showing pronounced non-linear response as observed also by the decrease of the echo amplitude. Furthermore, for the small particles the third harmonic is gradually increasing, whereas for the big particles there is a more abrupt increase followed by a steep drop. This phenomenon has been explained in detail in section 4.3 of this thesis. By the time that the yielding point is reached, the third harmonic is still increasing for the small particles until it’s maximum value, wherein for the big particles a drop is observed and the echo amplitude has already been fully decorrelated in both cases. It should also be noted that small particles yield faster than the bigger particles. After the total decorrelation of the echo amplitude the system becomes a liquid as seen from the Dynamic strain sweep also.

Volume fraction dependence:

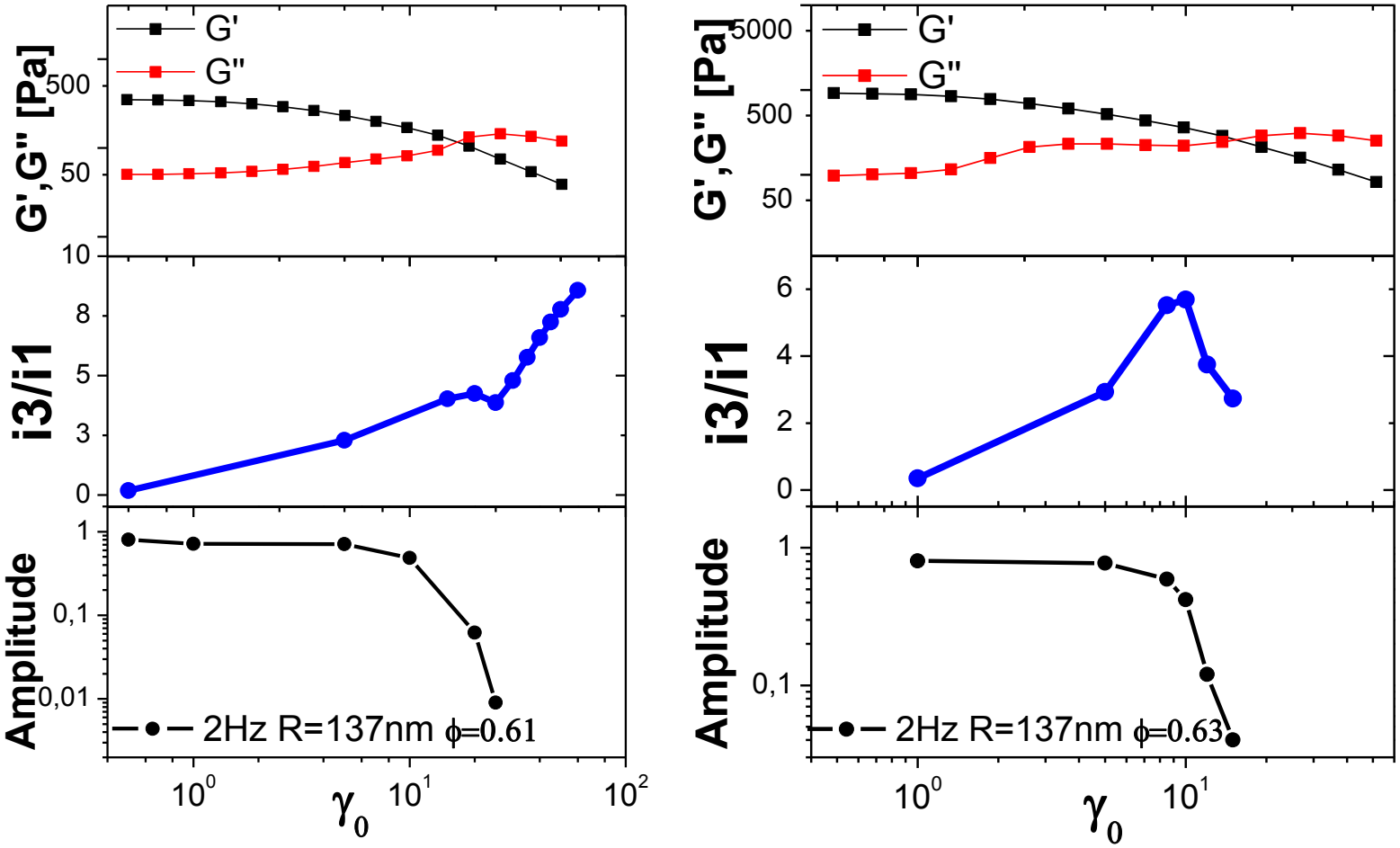

Figure 4.4.15: *Comparison of the elastic G' and viscous G'' modulus, with the third harmonic response and echo amplitude decay for small particles (R=137nm) with 2Hz frequency for φ=0.61 (left) and for φ=0.63 (right).*

With figure *4.4.15* the volume fraction dependence for the small particles is illustrated. Initially, concerning the rheological response, in the case of higher volume fraction the system yields faster. Hence, the yielding process is more abrupt compared to the smaller volume fraction where it is a more gradual process. For φ=0.63 a third harmonic drop is observed, similar to what was observed for the big particles in figure *4.4.15* however, this occurs before the yielding point and the echo amplitude is starting to dramatically decorrelate at this point. Finally, when the yielding point is reached the third harmonic drops to a minimum and the echo amplitude drops to zero.

Frequency dependence:

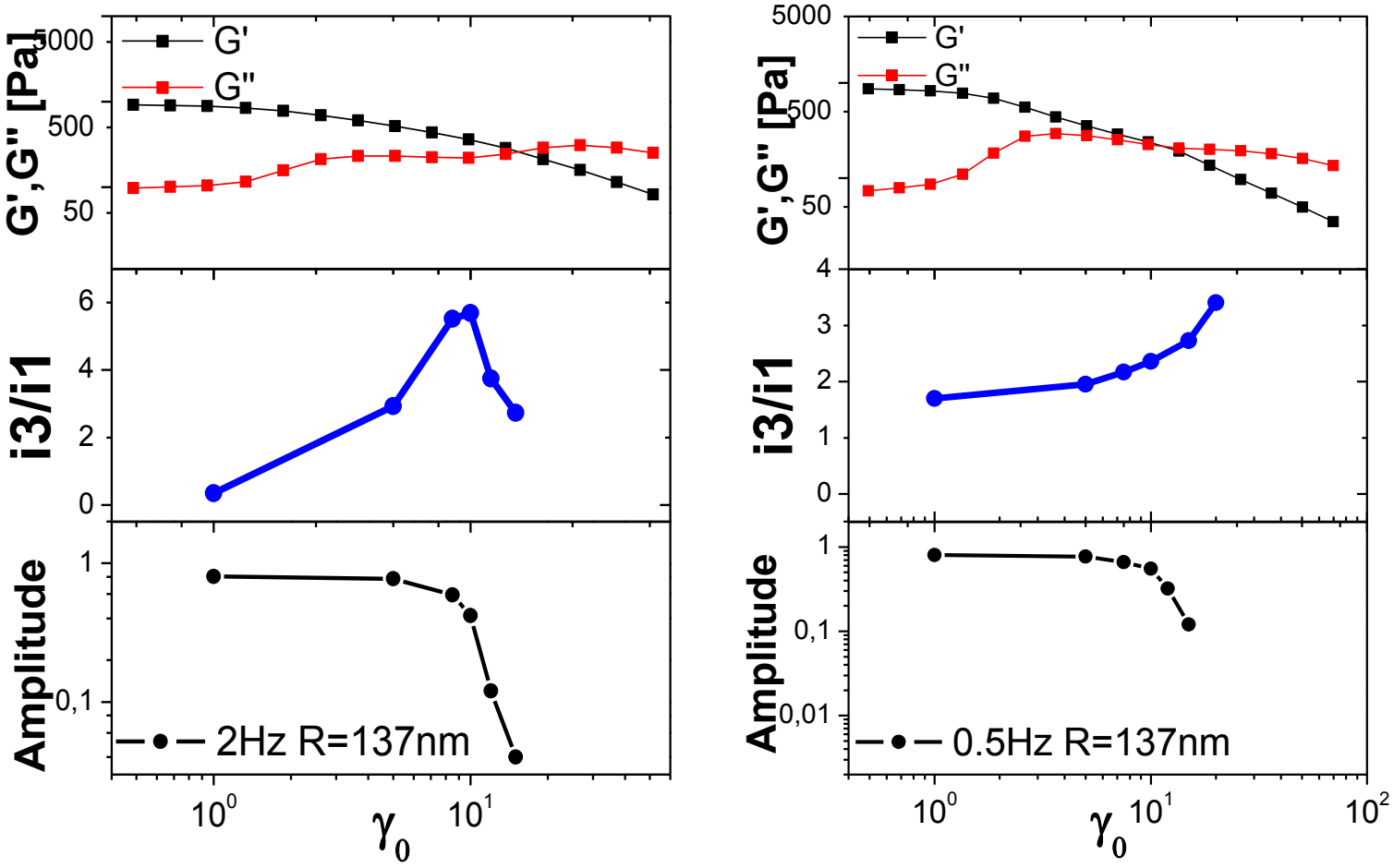

Figure 4.4.16: *Comparison of the elastic G' and viscous G'' modulus, with the third harmonic response and echo amplitude decay for small particles (R=137nm) φ=0.63 with 2Hz frequency (left) and 0.5Hz frequency (right).*

Figure *4.4.16* sheds some light on the frequency dependence of the small particles. Firstly, for the 0.5Hz frequency the system yields faster revealing the importance of Brownian motion which is dominant on low Peclet for the system's restructuring. Furthermore, the third harmonic is increasing with increasing strain until the yielding point where the maximum value is reached. On the other hand, there is a drop for the 2Hz as shown also in figure *4.4.15*. What is more for 0.5Hz frequency when the system yields the echo amplitude has almost been fully decorralated, as witnessed for the 2Hz also.

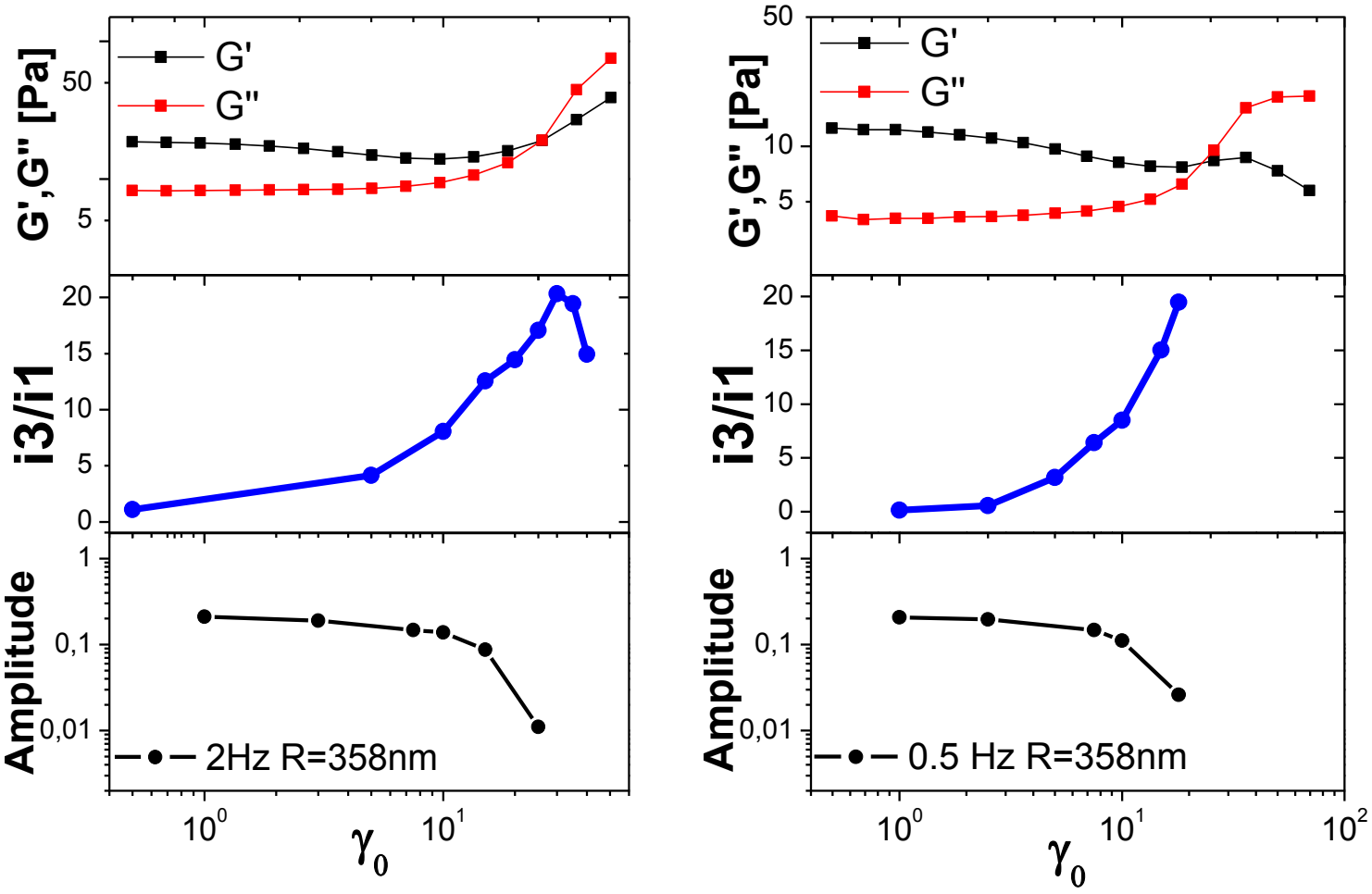

Figure 4.4.17: *Comparison of the elastic G' and viscous G'' modulus, with the third harmonic response and echo amplitude decay for big particles (R=358nm) φ=0.61 with 2Hz frequency (left) and 0.5Hz frequency (right).*

Figure *4.4.17* points out the frequency dependence of the big particles. Firstly, the system yields almost at the same strain, showing that in high Peclet where shear is dominant the particles are not affected by frequency as much as with the small particles where Brownian motion dominates. Furthermore, for 0.5Hz at the yielding point the third harmonic drop does not occur and in contrast with 2Hz a maximum is reached. Nevertheless, when the system yields the echo amplitude for both cases totally decorrelates.

Peclet regime dependence:

Pe_ω = 0.162 **Pe_ω = 0.649**

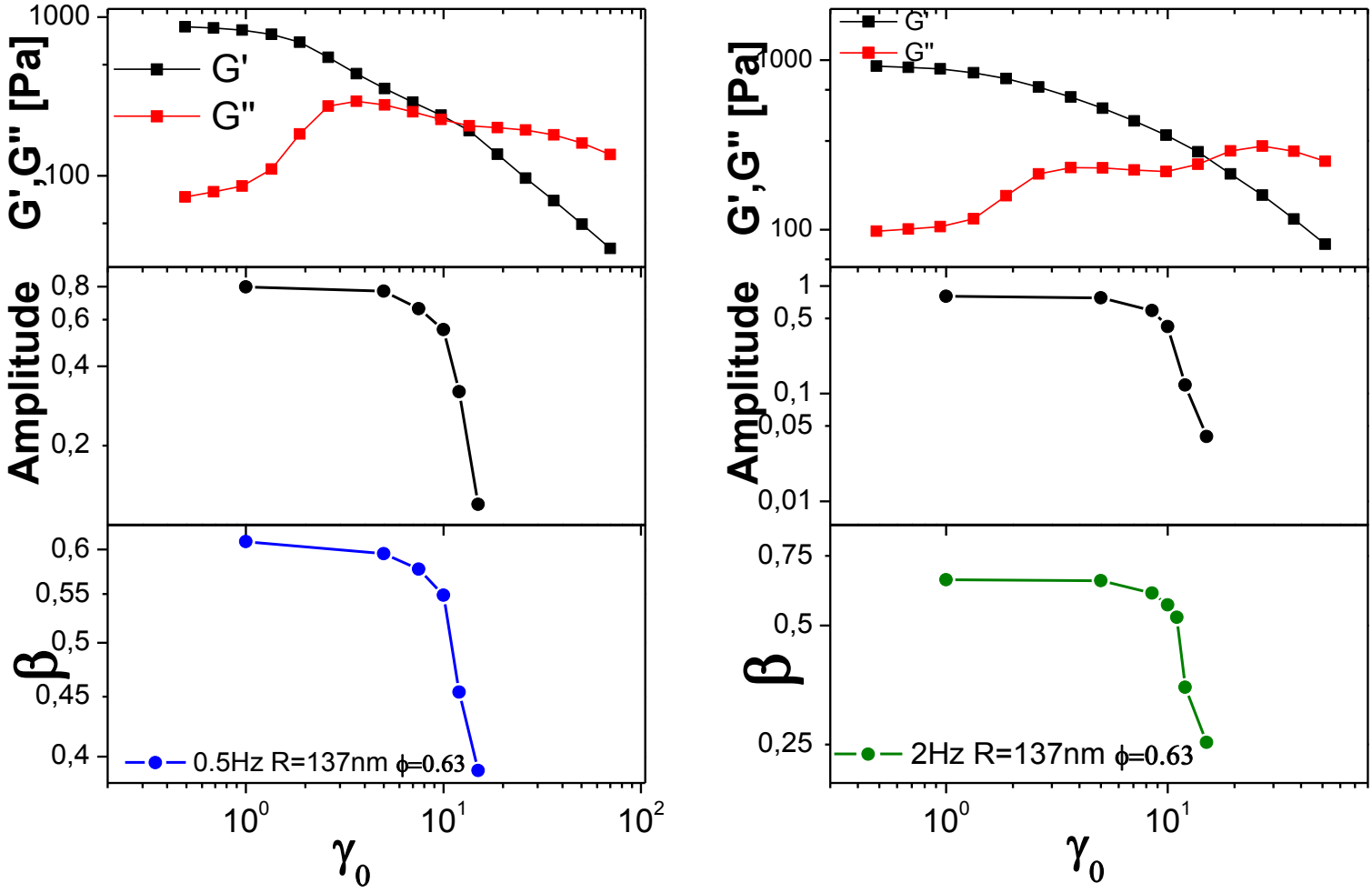

Figure 4.4.18: *Comparison of the elastic G' and viscous G'' modulus, with the echo amplitude decay and beta exponent for small particles (R=137nm) φ=0.63 with 0.5Hz frequency (left) and 2Hz frequency (right).*

Pe_ω = 2.95 **Pe_ω = 11.74**

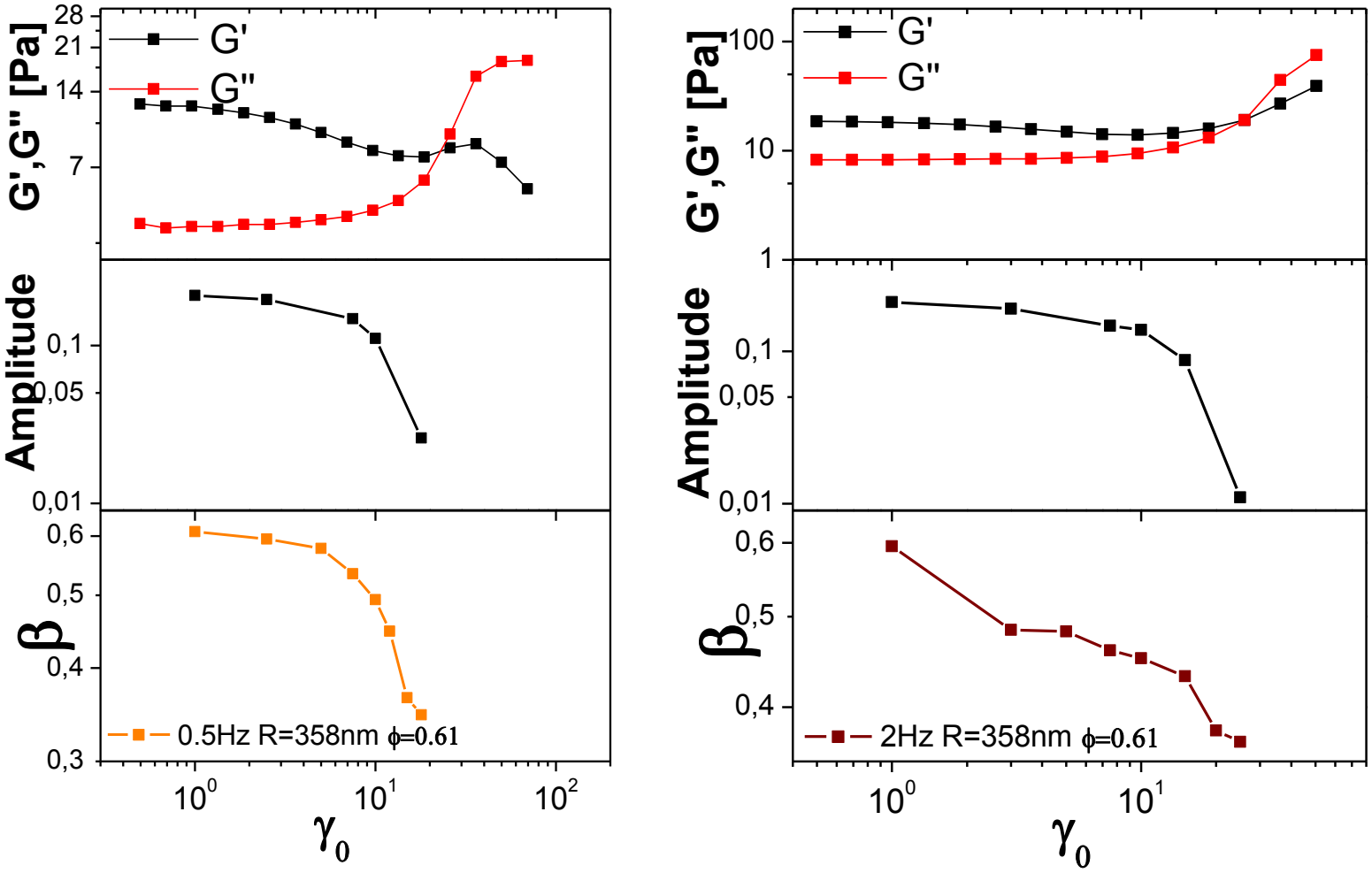

Figure 4.4.19: *Comparison of the elastic G' and viscous G'' modulus, with the echo amplitude decay and beta exponent for big particles (R=358nm) φ=0.61 with 0.5Hz frequency (left) and 2Hz frequency (right).*

The three different Peclet regimes ($Pe_\omega=\omega t_B$) can be observed in figures 4.4.18 and 4.4.19, starting from low Peclet (Pe_ω =0.162) where Brownian motion dominates, going to intermediate peclet (Pe_ω =0.649 and Pe_ω =2.95) where both mechanisms coexist and are comparable, with Brownian motion being significant for the first case (Pe_ω =0.649), and shear induced collision for the second case (2.95), until the high Peclet regime is reached where shear induced collision dominates (Pe_ω = 11.74). The yielding point (G'=G'') is observed in higher strain amplitude with increasing Peclet,

showing the different nature of Brownian motion yielding and shear induced collision yielding. Moreover, for every Peclet regime the echo amplitude is almost constant for the linear measurements showing solid-like behavior with reversible particle rearrangements, whereas with increasing strain amplitude for the non-linear measurements a liquid like behavior is contemplated with irreversible particle rearrangements until the yielding point where the system becomes fully fluidized and system correlation is lost. Furthermore, the beta exponent ranges between 0.6-0.25 and a gradual decreasing trend is observed for all Peclet regimes with the exception of high Peclet regime where the decrease is more abrupt.

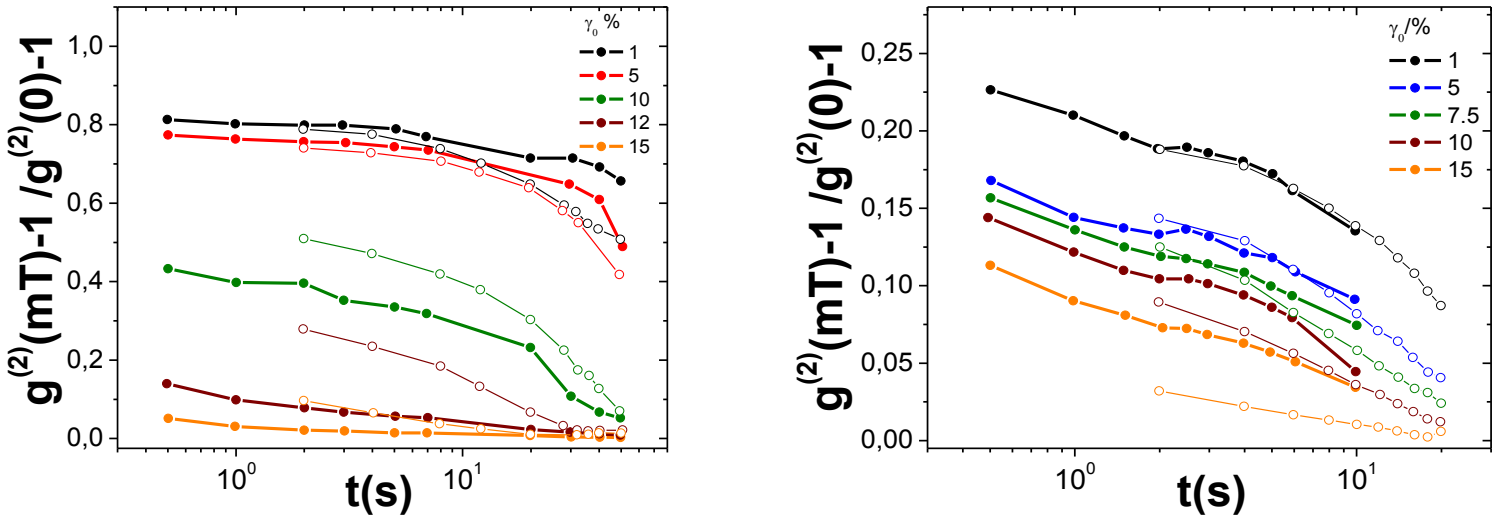

Figure 4.4.20: *Light scattering echo peak height with time for 0.5Hz (open symbol) and 2Hz (Closed symbol) frequency, for small particles R=137 (left) and big particles (right)*

In both particle sizes, almost the same amplitudes are observed for the same applied strain amplitude until 5%. For larger strain amplitude there is a difference between the two frequencies, with 2Hz showing a bigger decrease in the correlation function. As a result, this means that frequency does not affect the drop of the correlation function as much as strain amplitude does until 5% strain. For larger strain amplitude even more irreversible rearrangements are induced for 2Hz frequency showing more pronounced non-linear effects for larger Peclet regime. Under these circumstances strain amplitude is mostly responsible for the irreversible particle rearrangements, while frequency affects only in higher Peclet regime as manifested by figure 4.4.20.

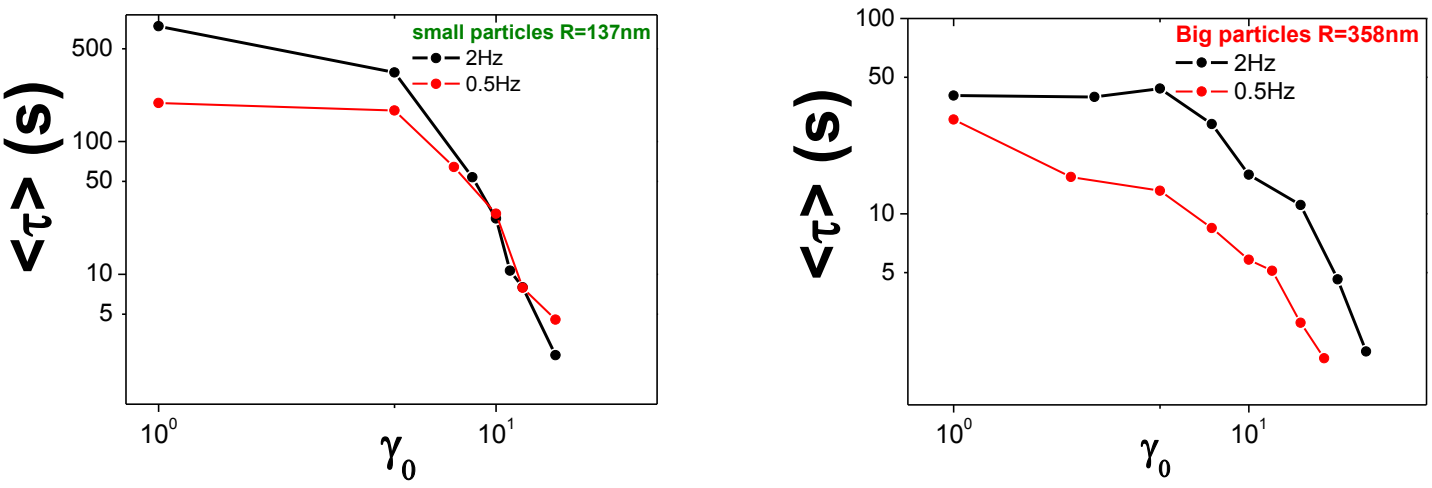

Figure 4.4.21: Average relaxation time with strain amplitude for small particles R=137nm (left) and big particles (right), for 2Hz and 0.5Hz frequency.

The average relaxation time is given by the relationship $<\tau>=\tau\Gamma(1/\beta)/\beta$, where τ is the fitting time (material dependent) , $\Gamma(1/\beta)$ is the gamma function , where:

$\Gamma(1/\beta) = \int_0^\infty x^{1/\beta-1}e^{-x}\,dx$. A decrease in both cases is observed with increasing strain amplitude for both particle sizes and both frequencies as contemplated by figure 4.4.21. For the small particles, the average relaxation time starts from 750 seconds dropping to 2 seconds, whereas for the big particles it starts around 50 seconds dropping again around 2 seconds. The relaxation time drop is more abrupt for the small particles (137nm) compared to the big particles (358nm) which is more gradual, this is an indication of a faster system relaxation which is also broader as observed by the beta exponent drop in figure 4.4.11.

Chapter 5: Conclusions

In this work rheological measurements and LS Echo were performed in order to gain a better understanding of the two mechanisms found in repulsive colloidal glasses: 1) Brownian motion and 2) Shear induced collision. For this reason two different particle sizes were used: small (137nm) and big (358nm) in order to gain access to the regimes where each mechanism dominates over the other. To begin from the correlation function analysis, a drop in the first echo was observed indicating shear induced rearrangements with increasing strain amplitude, while frequency does not affect as much. This can also be confirmed from the rheological measurements: 1) non-linear behavior of G' and G'' 2) increase in the third harmonic and 3) change from the linear elliptic shape of the lissajous plots to the parallelogram shape for small particles and double concave for big particles. The same behavior was observed even when the Brownian contribution was taken out of the correlation function (P_T/P_0T).

Starting from the linear regime for φ=0.61 both particles show an increased elastic modulus G' with increasing frequency while at the same time the viscous modulus minimum is characteristic of colloidal gels and glasses. The characteristic time a particle needs to explore it's cage is related to the minimum of G''. For small particles G' and G'' values are much higher than in big particles, because there is a direct proportionality to the thermal energy K_BT. Turning to the non-linear regime in both particle sizes shear thinning behavior is observed where G' decreases and G'' increases at the same time, showing that the system is becoming fluidized. Moreover, upon further incretion of strain amplitude the big particle system becomes shear thickening which is signified by a gradual G' increase.

To illustrate the rheological response furthermore, the Lissajous-Bowdich plots were observed where the big particles reveal the transition from the low Peclet rectangular shape Lissajous plot that shows both elastic and plastic responses to the high Peclet regime where an ellipsoid with a double concave distortion shape is being contemplated. For the small particles there is a transition from a linear visco-elastic behavior (regular elliptical shape) of low strains, to a distorted parallelogram pattern instead. [3]

In addition to rheology, Fourier transform quantifies the amplitude of non-linearity by introducing the dominant third harmonic. Naturally, for the big particles a more anisotropic particle cage is formed due to fewer particle collisions as quantified by the sudden drop of the third harmonic, therefore allowing flow with less stress compared to the small particles where Brownian motion relaxes shear-induced structural anisotropy more efficiently. [3] Above all, for the big particles this response is contemplated by the third harmonic drop.

Furthermore light scattering echo monitors the elastic and plastic behavior of the colloidal particles by directly following their motions. All $g^{(2)}(mT) - 1$ functions show an initial decay attributed to the short-time Brownian-dynamics and a decay at longer times which is associated to the shear-induced plastic rearrangements of the glass. For low strains, the material responds elastically almost like a solid and no significant structural rearrangements are observed. On the other hand, for higher strain amplitude the material responds like a liquid and irreversible structural rearrangements occur. The transition from Brownian activated yielding, where particles under shear with the aid of thermal motion escape their cages to the shear induced collision cage breaking at higher frequencies is directly linked to the stronger irreversible particle rearrangements and decreasing critical yielding strain at lower frequencies.

Correspondingly, thermal fluctuations evolve in a two-step process in highly concentrated suspensions where particles are restricted in cages formed by their neighboring particles β relaxation which corresponds to the fast motion of particles inside the cage, in contrast with the α relaxation where an extremely slow diffusion at longer distances takes place corresponding to cage breakdown [4], [5]. What is more, the shear induced decay of the relative first echo can elucidate the particle rearrangements due to shear showing pronounced effects above γ_o=10% for both particle sizes.

Usually, a reduction in $\frac{P(T)}{p_0(T)}$ can be caused by two factors: 1) a decrease of the non-ergodic plateau and/or 2) a long-time decay under shear acceleration [16]. In general, the higher the applied frequency the faster particles will relax due to the fact that they cannot relax with their intrinsic relaxation.

Moreover, in order to ensure the validity of our measurements the inverse half width at half height of the first echo was introduced (the inverse initial decay rate $\Gamma^{-1)}$. This linear proportionality is observed and besides indicating the absence of wall-slip and shear banding effects, it also proves the reproducibility of our experiments. [6]

Also, from the KWW stretched exponential fit of the correlation function, the average relaxation time and beta exponent were calculated giving a deeper insight in the system response for both particle size in different Peclet regimes. Not only was a decreasing average relaxation time observed with increasing strain amplitude indicating that the system relaxes faster, but also the decrease of beta exponent with increasing strain amplitude revealed a broader spectrum of relaxation times. What is more, the different Peclet regimes available were thoroughly studied with the comparative plots in order to highlight the difference between the two known mechanisms. Starting from low Peclet (Pe_ω =0.162) where Brownian motion dominates and (Pe_ω =0.649) where shear induced collision is somewhat comparable, going to intermediate (Pe_ω =2.95) where there is a stronger competition between Brownian motion and shear induced collision, until the high Peclet is reached (Pe_ω =11.74) where shear induced collision totally dominates. There is no visible difference observed starting from low to high strain amplitude: The correlation function decays fully by the time the yielding point is reached (G'=G'') in the same way for all Peclet regimes available. To summarize, this might happen due to the slight difference in particle size and frequency applied, leaving an open question as to whether even larger particles and frequency applied could highlight the differences between the two mechanisms even more.

References

[1] Randy H. Ewoldt, A. E. Hosoi, and Gareth H.McKinley J.Rheol 52(6), 1427-1458 November-December (2008)

[2] Wilson Poon, Peter Pusey, and Henk Lekkerkerker Physics World, (1996)

[3] N.Koumakis, J.F. Brady, and G.Petekidis PRL 110, 178301 (2013)

[4] W.Van Megen and P.N. Pusey , Phys.Rev. A 43, 5429 (1991)

[5] W.Van Megen and S.M. Underwood, Phys. Rev. E 49, 4206 (1994)

[6] G.Petekidis, A.Moussaid, and P.N Pusey PRE 66, 051402 (2002)

[7] Pusey, P.N, J. Phys. (Paris) 48. (1987)

[8] Bartlett, P., "A geometrically –based mean-field theory of polysdisperse hard-sphere mixtures." J.Chem. Phys. 107(1), 188-196

[9] N.Koumakis, A.Pamvouxoglou, A. S. Poulos and G.petekidis, "Direct comparison of the rheology of model hard spheres and soft particle glasses." Soft Matter. 2012.8. 4271-4284.

[10] T.G. Mason and D. A. Weitz. "Linear viscoelasticity of colloidal hard sphere suspensions near the glass transition", Phys.Rev. Lett ., 1995, 75(14), 2770-2773.

[11] N.Koumakis (2007) "Shear induced crystallization of a colloidal glass". Master Thesis

[12] Graham, M.D., "wall slip and the nonlinear dynamics of large amplitude oscillatory shear flows", J.Rheol .39(4), 697-712 (1995).

[13] Abhijit P. Deshpande "Techniques in oscillatory shear rheology"

[14] Hebraud, P., F. Lequeux, J.P. Munch, and D.J. Pine, "yielding and rearrangements in concentrated emulsions," Phys. Rev. E 78, 4657 (1997).

[15] Höler, S., S. Cohen –Addad, and H.Hoballah, "Periodic nonlinear bubble motion in aqueous foam under oscillating shear strain," Phys.Rev Lett. 79, 1154 (1997).

[16] M. Laurati, S.U. Egelhaaf , and G.Petekidis, "Plastic rearrangements in colloidal glasses investigated with LAOS and Echo-DWS.

[17] N.Koumakis (2011) " A study of the effects of interparticle interactions on the dynamics, rheology and aging of colloidal systems out of equilibrium" PHD thesis.